# TEMPORAL PATTERN OF SYNAPTIC ACTIVATION DIFFERENTIALLY AFFECTS PLASTICITY IN NORMAL AND INJURED BRAIN

Quentin S. Fischer[a,b,*], Djanenkhodja Kalikulov[a,b], Gonzalo Viana Di Prisco[b,1], Carrie A. Williams[a], Philip R. Baldwin[b,2] and Michael J. Friedlander[a,b,c,d,e*]

[a]*Fralin Biomedical Research Institute at VTC, Center for Neurobiology Research, 2 Riverside Circle, Roanoke VA 24016 USA*

[b]*Dept. of Neuroscience, Baylor College of Medicine, 1 Baylor Plaza, Houston TX 77030 USA*

[c]*Department of Biological Sciences, Virginia Tech, Derring Hall, 926 W. Campus Dr., Blacksburg VA 24060 USA*

[d]*Department of Psychiatry & Behavioral Medicine, Virginia Tech Carilion School of Medicine, 2 Riverside Circle, Roanoke VA 24016 USA*

[e]*Faculty of Health Sciences, Virginia Tech, 2 Riverside Circle, Roanoke VA 24016 USA*

[*]*Corresponding authors. Fralin Biomedical Research Institute at VTC, 2 Riverside Circle, Roanoke VA 24016 USA. Email addresses: fischerq@vtc.vt.edu (Q. Fischer), friedlan@vtc.vt.edu (M. Friedlander)*

[1]*Present address: Dept. Pharmacology & Toxicology, Indiana University School of Medicine, 320 W. 15th St., NB-400, Indianapolis, IN 46202 USA. Email address: gvianadi@iu.edu*

[2]*Present address: Dept. Biochemistry & Molecular Pharmacology, Baylor College of Medicine, 1 Baylor Plaza, Houston TX 77030 USA. Email address: Philip.Baldwin@bcm.edu*

**Abstract**

*Background*. Neurostimulation is increasingly used as a therapeutic intervention. Alterations in strength of synaptic connections (plasticity: long-term potentiation, LTP; long-term depression, LTD) are sensitive to the frequency of synaptic conditioning. However, little is known about the contribution of the temporal pattern of synaptic activation to plasticity in normal or injured brains.

*Objective*. We explore interactions of temporal pattern and frequency in normal cortex and after mild traumatic brain injury (mTBI) to understand the role of temporal pattern in healthy brains and inform therapies to strengthen or weaken circuits in injured brains.

*Methods*. Whole-cell (WC) patch-clamp recordings of evoked postsynaptic potentials (PSPs) and field potentials (FPs) were made from layer 2/3, in response to stimulation of layer 4, in acute cortical slices from control (naive), sham, and mTBI rats. We compared plasticity induced by different stimulation paradigms, each consisting of a specific frequency (1 Hz, 10 Hz, or 100 Hz), continuity (continuous or discontinuous), and temporal pattern (perfectly regular, slightly irregular, or highly irregular).

*Results*. Within each stimulation paradigm plasticity for individual cells was heterogeneous. Highly irregular stimulation produced net LTD in controls, but net LTP after mTBI (except for 100 Hz paradigms). The kinetic profile of responses during conditioning was predictive of plasticity outcome under some conditions. Simultaneous WC and FP recordings had highly correlated plasticity outcomes.

*Conclusions*. These experiments demonstrate that temporal pattern contributes to induction of synaptic plasticity in the normal brain and that contribution is altered by mTBI in ways that may inform brain stimulation therapies.

**Keywords**

Neural coding, brain stimulation, electrophysiology, traumatic brain injury, long-term potentiation, long-term depression

**Highlights**

- Each temporal pattern of stimulation produced heterogeneous plasticity outcomes
- Highly irregular stimulation produced LTD in controls, but LTP after mild TBI
- The kinetic profile of conditioning responses was predictive of plasticity outcome
- Whole-cell and field potential measurements of plasticity were highly correlated

**Abbreviations**

ACSF, Artificial cerebrospinal fluid

ANOVA, analysis of variance (one-way)

CCI, Controlled cortical impact

CV, Coefficient of variation

Dunn's test, Dunn's method for multiple comparisons

Fisher's LSD test, Fisher's least significant difference method for multiple comparisons

FP, Field potential

ISI, Interstimulus interval

Kruskal-Wallis test, Kruskal-Wallis one-way ANOVA on ranks

L2/3, Layer 2/3

L4, Layer 4

LTD, Long-term depression

LTP, Long-term potentiation

mTBI, mild traumatic brain injury

MWU test, Mann-Whitney U test

NC, No change

PSP, Postsynaptic potential

SIU, Stimulus isolation unit

WC, Whole-cell

HW, half width at half height

DT, decay time

RT, rise time

## 1. **Introduction**

A wide variety of neurological and psychiatric effects can result from brain injury such as mTBI [1–6]. The capacity of the brain to adapt to injury and undergo restorative plasticity throughout the lifespan is well documented [7–14]. Up- and down-regulation of the strength of synaptic transmission such as LTP and LTD represent processes implicated as biological substrates of learning and memory [15–27]. Such changes have been observed throughout the brain including in the: hippocampus [28–31], visual cortex [32–34], olfactory cortex [35,36], somatosensory and motor cortices [37–39], striatum [40,41] and cerebellum [42,43]. LTP and LTD are also implicated in refinement of synaptic connections during brain development and in functional reorganization of neuronal networks throughout the lifespan [21,44–50], after brain injury [51–56], and during neuro-rehabilitation for brain injury or disease [57–63]. It is of interest to learn whether these synaptic plasticity processes may be selectively evoked to facilitate a compensatory re-balancing of the relative strengths of particular synaptic pathways after mTBI and thus become part of the therapeutic toolbox for restoring functionality [64–66]. Moreover, with availability of various neurostimulation technologies such as: deep brain stimulation [67,68], transcranial focused ultrasound [69,70], transcranial magnetic stimulation [71–73], transcranial direct current stimulation [74,75], and more [76], to treat conditions such as Parkinson's disease [77–79], Alzheimer's disease [80–82], seizure disorders [83–85] and major depression [86–89], there is value in better understanding the effects of these interventions on synaptic plasticity in a well-controlled experimental environment.

Although, clinical uses of deep brain stimulation have begun to take into account the effects of temporal pattern [90–92], most experimental approaches to studying the induction mechanisms for LTP and LTD hold temporal patterns regular and constant, with a brief period of high frequency

afferent stimulation [93,94], a protracted period of low frequency presynaptic stimulation [31,95] or a series of conjunctions of temporally coincident pre- and post-synaptic activation [96–98]. While varying stimulation frequency, these protocols maintain a regular interval between each stimulus such that the temporal pattern of presynaptic stimulation is invariant (i.e. all interstimulus intervals, ISIs, are equal). These temporally regular epochs of synaptic stimulation are useful for experimental paradigms and have been widely applied particularly in isolated *in vitro* experimental preparations where the neurons are usually quiescent until stimulated. However, *in vivo* many neurons exhibit ongoing activity, continuously receiving synaptic inputs, many of which are evoked by presynaptic action potentials [99–103]. Moreover, the temporal pattern of the action potentials and subsequent evoked synaptic activity is often highly irregular with varying distributions of ISIs [104–109]. Thus, it is important to understand the contribution of temporal pattern (vs. frequency alone) of evoked synaptic activity *per se* to the induction of synaptic plasticity in the normal brain and whether there are different temporal pattern requirements for accessing the downstream synaptic plasticity signaling cascades after mTBI.

Since the neocortex is often subjected to the effects of mTBI and the synaptic circuitry of the visual cortex is well characterized, we chose this area to evaluate the role of the temporal pattern of evoked synaptic activity. In particular, we were interested to learn whether the major synaptic drive from the neurons of the primary thalamic input zone (layer 4, L4), onto the layer 2/3 (L 2/3) pyramidal projection neurons that transmit information over long distances between cortical areas, react differently to variations in the temporal pattern of conditioning inputs in the normal brain and after mTBI. Since the parameter space to explore the distributions of ISIs and frequencies is vast, we focused on a few synaptic stimulation frequencies known to play a role in plasticity in neocortex (1 Hz, 10 Hz and 100 Hz), three temporal pattern distributions (perfectly

regular where all ISIs are identical with a coefficient of variation or CV = 0.0, a slightly irregular Gaussian distribution of ISIs with a CV = 0.2, and a highly irregular Poisson distribution of ISIs with a CV = 1.0), and two types of conditioning epochs (continuous or discontinuous).

## 2. Methods

### *2.1. Animal use and experimental design*

All procedures were approved by the Institutional Animal Care and Use Committees of Virginia Tech or Baylor College of Medicine and followed the National Research Council's *Guide for the Care and Use of Laboratory Animals*. Male Long-Evans rats (HsdBlu:LE; Inotiv) were kept on a 12h light/12h dark schedule, and provided food and water *ad libitum*. At 8-9 weeks of age, rats were single housed and assigned to one of three treatment groups: control (naïve), sham (sham operated), or mTBI (controlled cortical impact, CCI). Two to three weeks later these animals were used in: behavioral, electrophysiological, and/or calcium imaging experiments (with experimenters blind to sham/mTBI status).

### *2.2. Mild traumatic brain injury model*

At 8-9 weeks of age the mTBI group received a CCI (using a well-established model) [110–112]. Briefly, 4h before surgery rats were started on an antibiotic regimen (Baytril 5 mg/kg, IM, *q.d.* x 3). Surgery was performed under isoflurane anesthesia (1–4%, in $O_2$). Rats were intubated, ventilated (TOPO, Kent Scientific), and end-tidal $CO_2$ was monitored (Capnograph 340, Harvard Apparatus). Animals were placed on a homeostatically controlled heating plate (TCAT-2DF, Physitemp) and mounted in a stereotaxic frame (Model 940, Kopf). The scalp was shaved, cleaned with alcohol and betadine, and incised to expose the skull. A 7 mm diameter craniotomy was made over the right parietal cortex immediately posterior to bregma and lateral to midline. A direct

lateral CCI (2.5 mm depth, 3.0 m/s velocity, 100 ms duration, angled at 45° from vertical) was delivered through intact meninges using a Benchmark stereotaxic impactor (Leica) with a modified 6 mm diameter spherical head. After the CCI, we administered a long-lasting analgesic (buprenorphine SR 1.2 mg/kg, SC; ZooPharm), the craniotomy and incision were repaired, and a topical antibiotic (Neosporin + pain relief, Johnson & Johnson) applied. Anesthesia was discontinued, the rat removed from the stereotaxic frame, extubated, and monitored until fully recovered. Shams received identical treatment except for the CCI.

*2.3. Righting reflex*

At 10-12 weeks of age (2-3 weeks after treatment: control, sham, or mTBI) the first cohort of 44 rats was examined to assess righting latency. Animals were placed in a transparent induction chamber (with 1L/min $O_2$). Anesthesia was induced by the addition of isoflurane (4% for 120 s). The rat was rapidly removed from the chamber and placed in a supine position. The time between the cessation of anesthesia and the recovery of the righting reflex (righting latency, defined as the time required for the rat to right itself to an upright posture standing on all four paws) was measured.

*2.4. Brain slice preparation*

At 10-12 weeks of age (2-3 weeks after treatment: control, sham, or mTBI) a second cohort of 316 rats was anesthetized with ketamine (75 mg/kg, IM) / xylazine (10 mg/kg, IM) then decapitated. The brain was rapidly removed and cooled for ~2 min in ice-cold cutting solution containing (in mM): 124 NaCl, 2 KCl, 3.5 $MgCl_2$, 0.2 $CaCl_2$, 1.25 $KH_2PO_4$, 26 $NaHCO_3$, 11 dextrose, and saturated with 95% $O_2$/5% $CO_2$ with a final pH of 7.4. Coronal slices (300 µm) were

prepared from the right visual cortex (ipsilateral to the mTBI) using a vibratome (VT1000P, Lecia) and placed in artificial cerebral spinal fluid (ACSF) containing (in mM): 124 NaCl, 2 KCl, 2 $MgCl_2$, 2 $CaCl_2$, 1.25 $KH2PO_4$, 26 $NaHCO_3$, and 11 dextrose and saturated with 95% $O_2$/5% $CO_2$ with a final pH of 7.4. Slices were incubated in ACSF at 33 ± 1ºC for 20 min and then at room temperature for > 40 min prior to recording.

*2.5. Electrophysiology: recording*

For recording, slices were transferred to a submersion chamber perfused with 3 ml/min of ACSF at 33±1ºC. L2/3 pyramidal neurons were visualized using an upright microscope (Axio Examiner.D1; Zeiss) equipped with a W Plan-Apochromat 40x water immersion objective and configured for DGC microscopy. A bipolar stimulating electrode (FHC #30213) was placed in L4. Glass micropipettes (Garner KG-33, OD 1.5 mm, ID 1.12 mm; A-M Systems) were pulled on a vertical puller (PC-10, Narishige) to make FP pipettes (1 ± 0.5 MΩ), or WC patch pipettes (4 ± 1 MΩ). FP pipettes were filled with ACSF and placed superficially in L2/3. WC patch pipettes were filled with pipette solution (containing in mM: 115 K-gluconate, 20 KCl, 10 Hepes, 4 NaCl, 4 Mg-ATP, 0.3 Na-GTP, and 4 phosphocreatine-Na, pH 7.4, 280-290 mOsm) and placed in L2/3 (~100 µm deep to the FP pipette). Biocytin (0.5%; Sigma-Aldrich) was added to the WC patch pipette solution to allow post-hoc identification of patched cells (only pyramidal cells located in L2/3 were analyzed).

All recordings were made using a MultiClamp 700B amplifier, digitized at 20 kHz with a Digidata 1440A, and collected and analyzed with pCLAMP 10 software (Clampex and Clampfit; Molecular Devices). Recordings of evoked FP and WC PSP amplitudes were measured as the difference between baseline and peak. Recordings with unstable pre-conditioning response

amplitudes (linear best fit of PSP, or FP, peak amplitudes with an $r^2 > 0.2$) were discarded. WC recordings with membrane potentials more positive than -60 mV, high access resistance (> 40 MΩ, or > 20% of the membrane resistance for that cell), or a > 20% decrease in input resistance were discarded. The intrinsic firing properties of patched cells were tested by injecting a 100 ms depolarizing current pulse and cells that did not exhibit regular spiking typical of excitatory cells [113,114] were discarded. Only one recording was made from each slice, so that a single stimulation protocol was applied in each case.

*2.6. Stimulation protocols*

Afferent stimulation consisted of constant current square wave pulses 100 µs in duration and 30-500 µA in amplitude (~40% of the maximal PSP response) output by a stimulus isolation unit (SIU; A365, World Precision Instruments). Stimulation was optimized to produce WC responses, but in some cases (~10%) was also sufficient to trigger FP responses which were recorded simultaneously. Pre-conditioning baseline recordings of evoked PSP (and FP) peak amplitudes were made at a stimulation frequency of 0.1 Hz for 10 min. This was followed by a 90 or 900 s period of synaptic conditioning, consisting of 900 pulses at 1 Hz, 10 Hz, or 100 Hz. Conditioning stimulation was either continuous (1 Hz for 900 s, or 10 Hz for 90 s; Fig. 1A-B) or discontinuous (9 epochs of 100 pulses each at 10 Hz or 100 Hz, separated by 8 equal rest intervals consisting of probe trials at 0.1 Hz, with a total duration of 900 s; Fig. 1C). We included the discontinuous paradigms since continuous stimulation at higher frequencies (10 Hz, 100 Hz) might induce presynaptic fatigue that could interact with long-term synaptic plasticity [115,116]. Post-conditioning evoked PSP (and FP) peak amplitudes were evaluated at 0.1 Hz for a period of 20 min. Conditioning stimulation was delivered with one of three temporal patterns: perfectly regular

(all ISIs equal, coefficient of variation = 0, CV 0.0; Fig. 1D-E), slightly irregular (Gaussian distribution of ISIs, CV 0.2; Fig. 1F-G), or highly irregular (Poisson distribution of ISIs, CV 1.0; Fig. 1H-I) each with the same mean frequency. Conditioning stimulation was generated using MatLab (MathWorks), transformed with a digital analog converter (BNC 2090A, National Instruments), triggered with a pulse stimulator (Master 9, A.M.P.I.), and output via the SIU, allowing us to control the precise: frequency, continuity and temporal pattern of stimulation.

*2.7. Stimulation: pattern generation*

Stimulus patterns were generated by creating ISIs according to the family of distributions given by:

$$P(t) \propto e^{-t^2/2\eta^2} e^{-t/\tau_d} \theta(t > \tau_R) \qquad (1)$$

where $\tau_R$ is the refractory period, and $\eta$ (>0) and $\tau_d$ are temporal parameters that govern the single peak of the distribution. For a perfectly regular distribution, we had $-\tau_d/\eta >> 1$, and for a highly irregular distribution $\eta/\tau_d >> 1$. We solved for the parameters $\eta$ and $\tau_d$, to yield a desired mean, m, and standard deviation (std) or coefficient of variation (CV):

$$\frac{\mathrm{std}^2}{\mathrm{m}^2} = \frac{Q(w)^2 + 2wQ(w) - 2}{2(1 - wQ(w))^2}, \qquad (2)$$

$$m = \tau_R + \left(\eta\sqrt{2}\right)\left(\frac{1 - wQ(w)}{Q(w)}\right), \qquad (3)$$

where $Q(w) \equiv \sqrt{\pi}\ \mathrm{erfcx}(w)$, and $w \equiv \frac{\eta}{\tau_d\sqrt{2}} + \frac{\tau_R}{\eta\sqrt{2}}$. Since equations (2) and (3) are monotonic, one can invert the equations to find $\eta$ and $\tau_d$ in terms of m and std. Thus, it was possible to change a set of ISIs at one CV to a related set of ISIs at another CV. The cumulative distribution function corresponding to the event probability distribution function given by equation (1) above is:

$$\mathrm{cdf}(t) = 1 - \frac{\mathrm{erfc}(w + (t - \tau_R) / (\eta\sqrt{2}))}{\mathrm{erfc}(w)}. \quad (4)$$

We randomly assigned numbers drawn uniformly on the unit interval to ISIs in the following way. For each random number, r, we inverted equation (4) to find a *t* that represented an ISI affiliated with a given mean and CV. By specifying a different mean and CV (and therefore different η and $\tau_d$, or equivalently, different η and *w*) in equation (4) we derived related sets of ISIs, using a single set of random numbers.

*2.8. Electrophysiology: data analysis*

We measured evoked PSP (or FP) peak amplitudes during the last 5 min of pre- and post-conditioning (using Clampfit) and calculated a post/pre ratio. We evaluated the effects of mTBI, as well as stimulus frequency, temporal pattern, and continuity on the induction of synaptic plasticity [which we defined as: LTD, a significant ($p < 0.05$, *t* test) decrease (≥ 10%) in post/pre ratios; LTP, a significant increase (≥ 10%) in post/pre ratios; or no change (NC), post/pre ratios that changed < 10% and/or were not significantly different ($p > 0.05$, *t* test)]. For these same time periods (the last 5 min of pre- and post-conditioning), we used Clampfit to calculate the average PSP: half width (at half height), rise time (10-90%) and decay time (90-10%); as well as the membrane potential and input resistance for each cell. Finally, we measured the kinetic properties of WC responses during the conditioning period. For continuous stimulation paradigms, we took all data points generated during the conditioning period and calculated an exponential and linear best fit, from which we determined the slope. For discontinuous stimulation paradigms, best fits were calculated for each of the nine stimulation sub-epochs and the slopes averaged. Further, we calculated the mean of all response amplitudes (average) as well as the average of the initial 10% (initial) and final 10% (final). For all recordings within a given stimulation paradigm, a simple

linear regression analysis was performed to determine the degree to which each of these factors (conditioning period: exponential slope, linear slope, average amplitude, initial amplitude and final amplitude) were correlated with plasticity outcome (post/pre ratio).

*2.9. Calcium Imaging*

In a subset of the WC patch experiments, the ratiometric calcium sensitive dye Fura-4F (100 μM, Thermo Fisher Scientific) was added to the pipette solution. The high dissociation constant of the dye at this concentration ensures it is permissive of plasticity [117,118]. Cells were illuminated using an ultra-high speed wavelength switching xenon arc lamp (Lambda DG-4 system; Sutter Instruments) controlled by a signal distribution box (SVB-1; Zeiss). Images were captured using an AxioCam HSm camera (Zeiss). Baseline somatic calcium concentrations were calculated as a ratio of bound to unbound calcium minus background (AxioVision, Zeiss) during the last five minutes of pre-conditioning.

*2.10. Histology*

After successful WC recordings, visual cortical slices were processed to verify pyramidal cell morphology and L2/3 location of recorded cells. Slices were fixed in 4% paraformaldehyde in 0.1 M phosphate buffer at 4ºC, then incubated overnight in an avidin-biotin-horseradish peroxidase complex at 4ºC with 0.1% Triton X-100 (Vector Elite; Vector Laboratories). The tissue was counterstained with cresyl violet and cover slipped with dibutyl phithalate (Electron Microscopy Sciences). Slides were visualized using a Zeiss AxioImager M2 microscope with a 40x oil immersion objective (EC PlanNeo-Fluar, Zeiss).

*2.11. Statistical Analyses*

A Shapiro-Wilk test (SigmaPlot, Systat Software) was used to determine if data were normally distributed. For normally distributed data, we used a *t* test (SigmaPlot or Microsoft Excel), or an ANOVA followed by Fisher's LSD method for multiple comparisons (SigmaPlot). For datasets with non-normal distributions, we used a Mann-Whitney U test (MWU, SigmaPlot), or a Kruskal-Wallis one-way ANOVA on ranks test (Kruskal-Wallis test, SigmaPlot) followed by Dunn's method for multiple comparisons (with Sidak correction; statskingdom.com/kruskal-wallis-calculator.html). Group data are presented as the mean ± standard error (SEM), unless otherwise noted. To assess whether specific characteristics of the conditioning stimulation responses were predictive of plasticity outcome, for each factor, we calculated a correlation coefficient and determined significance using simple linear regression (SigmaPlot). Differences were considered statistically significant when $p < 0.05$ (except for Dunn's tests which had a corrected alpha of 0.017).

## 3. Results

*3.1 Efficacy of our mTBI model*

To establish the efficacy of our CCI model for mTBI we used several independent methods. First, we used a behavioral measure, recovery of righting reflex, to assess motor and cognitive function in control, sham and mTBI rats. Righting latency was significantly impacted by treatment group ($p = 0.04$, ANOVA), and was longer in mTBI (247 ± 11 s) than in control (214 ± 9 s, $p = 0.04$) or sham (209 ± 13 s, $p = 0.02$, Fisher's LSD tests; Fig. 2A) groups. Note that for this and all subsequent figures we show control data in black, sham data in blue, and mTBI data in red. Second, we measured intracellular (somatic) calcium concentration in a subset of the L2/3 pyramidal

neurons used for our WC patch-clamp recordings. Intracellular calcium concentrations were significantly different between treatment groups ($p < 0.001$, Kruskal-Wallis test), and were higher in the mTBI (88 ± 4 nM) than in the control (63 ± 3 nM; $p < 0.001$) or sham group (61 ± 5 nM; $p < 0.001$, Dunn's tests; Fig. 2B). Third, we measured the intrinsic properties of this same subset of cells, and found that input resistance was significantly affected by treatment group ($p = 0.005$, Kruskal-Wallis test), being higher in mTBI (203 ± 12 MΩ) than in control (155 ± 9 MΩ, $p = 0.001$) or sham (149 ± 12 MΩ, $p = 0.008$, Dunn's tests; Fig. 2C) groups; while membrane potential did not differ ($p = 0.38$, Kruskal-Wallis test) between control (-70.1 ± 0.5 mV), sham (-71.1 ± 0.7 mV), or mTBI (-70.0 ± 0.6 mV; Fig. 2D) groups.

*3.2 Effect of temporal pattern and treatment condition on plasticity outcome: 1Hz continuous conditioning*

Having established the efficacy of our mTBI model we proceeded with WC patch-clamp experiments to investigate the possible role of temporal pattern on synaptic plasticity in acute slices from control, sham and mTBI rats. Figure 3 shows example recordings of evoked WC PSPs and time plots from individual WC recordings in response to 1 Hz continuous highly irregular stimulation (*cf.* Fig. 1A,H-I). Note the substantial decrease in post-conditioning PSP amplitude, indicative of LTD, in control and sham examples (Fig. 3A-B). In contrast, there was a substantial increase in post-conditioning PSP amplitude, indicative of LTP, in the mTBI example (Fig. 3C).

Grouped results for our WC recording experiments for the various frequencies, temporal patterns, and treatment groups are shown in the next four figures. Continuous stimulation at 1 Hz induced a net LTD in both control groups (Fig. 4A-C) and mTBI groups (Fig. 4D-E) under most conditions, with one exception—highly irregular stimulation (CV 1.0) in mTBI rats yielded a net

LTP (Fig. 4F). Temporal pattern (CV 0.0, CV 0.2, CV 1.0) had no effect on plasticity outcome in control groups ($p$ = 0.50, ANOVA; Figs. 4A-C,G). However, for mTBI groups, there was a significant difference in plasticity outcome between the three temporal patterns ($p$ = 0.002, Kruskal-Wallis test; Figs. 4D-F,H) with highly irregular stimulation showing significant potentiation (CV 1.0 vs. CV 0.0: $p$ = 0.007, CV 1.0 vs. CV 0.2: $p$ < 0.001; CV 0.0 vs. CV 0.2: $p$ = 0.19; Dunn's tests). Notably, within each of the six stimulation groups there was heterogeneity in plasticity outcomes among individual cells (Fig. 4G,H). Importantly, plasticity outcomes in control and mTBI rats were significantly different only when the temporal pattern was highly irregular (CV 1.0: $p$ = 0.008, MWU test; *cf.* Figs. 4C,F), but not when it was perfectly regular (CV 0.0: $p$ = 0.76, $t$ test; *cf.* Figs. 4A,D) or slightly irregular (CV 0.2: $p$ = 0.66, $t$ test; *cf.* Figs. 4B,E). Accordingly, for highly irregular stimulation (CV 1.0), we analyzed control, sham and mTBI groups ($p$ = 0.004, Kruskal-Wallis test; Fig. 4I). Pairwise comparisons (Dunn's tests) showed a significant difference between mTBI and control ($p$ = 0.002), and between mTBI and sham ($p$ = 0.002), but not between control and sham groups ($p$ = 0.49; Fig. 4I). The potentiation produced by highly irregular 1 Hz stimulation in mTBI rats reflects both an increase in the proportion (control = 18%, sham = 6%, mTBI = 47%) and magnitude (mean post/pre ratio in: control = 1.31, sham = 1.13, mTBI = 1.62) of LTP outcomes (Fig. 4I).

Additionally, highly irregular 1 Hz continuous stimulation differentially affected the evoked PSP shape indices (Supp. Fig. 1A) in controls, showing a significant decrease in decay time (DT; pre: 28 ± 2 ms, post: 24 ± 1 ms; $p$ = 0.03) and half width (HW, pre: 26 ± 3 ms, post: 22 ± 2 ms; $p$ = 0.03, paired $t$ tests; Supp. Fig. 1B), and this effect occurred primarily in the responses that underwent LTD (DT, pre: 28 ± 4 msec, post: 23 ± 2 msec, $p$ = 0.045; HW, pre: 26 ± 4 ms, post: 21 ± 2 ms, $p$ = 0.03; paired $t$ tests; Supp. Fig. 1C, *cf.* Supp. Fig. 1B,D). Shape indices in

shams showed a similar decrease in DT (pre: 35 ± 3 msec, post: 31 ± 4 ms; $p = 0.09$) and HW (pre: 32 ± 3 ms, post: 28 ± 3 ms; $p = 0.02$, paired *t* tests; Supp. Fig. 1B), which occurred only in responses that underwent LTD (DT, pre: 36 ± 4 ms, post: 30 ± 4 ms, $p = 0.03$; HW, pre: 32 ± 3 ms, post: 27 ± 4 ms, $p = 0.02$; paired *t* tests; Supp. Fig. 1C, *cf.* Supp. Fig. 1B,D). Interestingly, while the shape indices of the responses in the mTBI group as a whole did not change significantly after conditioning (DT, pre: 32 ± 3 ms, post: 35 ± 4 ms, $p = 0.49$; HW, pre: 30 ± 3 ms, post: 33 ± 3 ms, $p = 0.54$; paired *t* tests; Supp. Fig. 1B), among just the responses that underwent LTP they significantly increased (DT, pre: 32 ± 3 ms, post: 40 ± 6 ms, $p = 0.01$; HW, pre: 31 ± 3 ms, post: 36 ± 4 ms, $p = 0.01$; paired *t* tests; Supp. Fig. 1D, *cf.* Supp. Fig. 1B,C).

*3.3 Effect of temporal pattern and treatment condition on plasticity outcome: 10Hz continuous conditioning*

Continuous stimulation at 10 Hz produced a rapid rundown in PSP amplitudes, but was less likely to induce LTD, than 1 Hz continuous stimulation (*cf.* Figs. 5A-E, 4A-E). In particular, for controls, slightly irregular (CV 0.2) continuous stimulation produced LTD for 1 Hz, but NC for 10 Hz stimulation (*cf.* Figs. 4B, 5B; $p = 0.01$, *t* test); while after mTBI, perfectly regular stimulation (CV 0.0) induced LTD for 1 Hz continuous, but LTP for 10 Hz continuous stimulation (*cf.* Figs. 4D, 5D; $p = 0.05$, MWU test). Temporal pattern had no effect on plasticity outcome in control groups ($p = 0.58$, Kruskal-Wallis test; Figs. 5A-C,G). However, for mTBI groups, there was a significant difference in plasticity outcomes ($p = 0.002$, Kruskal-Wallis test; Figs. 5D-F,H) between slightly irregular stimulation (CV 0.2) which showed a shift toward LTD, and perfectly regular stimulation (CV 0.0) or highly irregular stimulation (CV 1.0) both of which showed a shift toward LTP ($p = 0.015$, or $p < 0.001$, Dunn's tests; Fig. 5H). Additionally, we found that 10 Hz

continuous stimulation (similar to 1 Hz continuous stimulation), produced significantly different plasticity outcomes for control and mTBI rats only when the temporal pattern of conditioning stimulation was highly irregular (CV 1.0: $p = 0.003$, MWU test; *cf.* Figs. 5C,F), but not perfectly regular (CV 0.0: $p = 0.35$, MWU test; *cf.* Figs. 5A,D) or slightly irregular (CV 0.2: $p = 0.10$, *t* test; *cf.* Figs. 5B,E). Accordingly, for highly irregular stimulation (CV = 1.0), we analyzed control, sham and mTBI groups ($p = 0.003$, Kruskal-Wallis test; Fig. 5I). Pairwise comparisons (Dunn's tests) showed a significant potentiation of responses in mTBI relative to control and sham groups ($p = 0.001$, $p = 0.004$, respectively), but no difference between controls and shams ($p = 0.30$). This potentiation reflected a change in both the proportion (control = 0%, sham = 12%, mTBI = 52%) and magnitude (mean post/pre ratio in: control = no LTP responses, sham = 1.24, mTBI = 1.56) of LTP outcomes. There were no effects of 10 Hz continuous conditioning on the shape indices of the PSP responses (data not shown).

*3.4 Effect of temporal pattern and treatment condition on plasticity outcome: 10Hz discontinuous conditioning*

For 10 Hz discontinuous stimulation protocols, the brief stimulation sub-epochs appeared to mitigate rundown of response amplitudes which we observed for 10 Hz continuous stimulation protocols (*cf.* Figs. 6A-F, 5A-F). Moreover, probe stimuli administered at 0.1 Hz during the rest periods (Figs. 6A-F, yellow symbols) showed that PSP amplitudes quickly recover, in most cases showing a brief period of post-tetanic potentiation, which suggests any synaptic fatigue induced by an individual sub-epoch of higher frequency stimulation is transitory. Interestingly, probe trail response amplitudes are sensitive to the temporal pattern of conditioning stimulation in control groups (depressed for CV 0.0 and CV 1.0, but potentiated for CV 0.2; *cf.* Figs. 6A-C) and mTBI

groups (potentiated for CV 0.0, neutral for CV 0.2, and potentiated for CV 1.0; *cf*. Figs. 6D-E). Notably, the continuity of 10 Hz conditioning stimulation influenced plasticity outcome and this was also dependent on temporal pattern. In controls, 10 Hz highly irregular stimulation (CV 1.0) induced significantly more robust LTD when stimulation was discontinuous rather than continuous ($p = 0.02$, MWU; *cf*. Figs. 5C, 6C). In mTBI groups, 10 Hz perfectly regular stimulation (CV 0.0) induced LTD for discontinuous stimulation, but LTP for continuous stimulation (p = 0.06 -- trend, MWU; *cf*. Figs. 5D, 6D).

For 10 Hz discontinuous (unlike 10 Hz continuous) stimulation there was a significant effect of temporal pattern between control groups ($p = 0.04$, Kruskal-Wallis test; Figs. 6A-C,G), as well as between mTBI groups ($p = 0.02$, Kruskal-Wallis test; Figs. 6D-F,H). Pairwise comparisons showed a significant effect of temporal pattern in controls with robust LTD in response to highly irregular stimulation (CV 1.0, Fig. 6C) compared to weak potentiation elicited by slightly irregular stimulation (CV 0.2, $p = 0.006$; Dunn's test; Figs. 6B,G). In mTBI groups, there was a significant difference between highly irregular (CV 1.0, Fig. 6F) and both: slightly irregular (CV 0.2, $p = 0.006$; Figs. 6E,H) and perfectly regular (CV 0.0, $p = 0.012$, Dunn's tests; Figs. 6D,H) stimulation. Moreover, control and mTBI groups differed only for highly irregular stimulation (CV 1.0, *cf.* Figs. 6C,F; $p < 0.001$, MWU test), and not for slightly irregular (CV 0.2, *cf*. Figs 6B,E; $p = 0.17$, MWU test) or perfectly regular (CV 0.0, *cf*. Figs. 6A,D; $p = 0.56$, *t* test) stimulation. Accordingly, for highly irregular stimulation (CV 1.0), we analyzed control, sham and mTBI groups ($p < 0.001$, Kruskal-Wallis test; Fig. 6I). Pairwise comparisons (Dunn's tests) showed a significant difference between treatment groups—with a robust shift toward LTP in mTBI relative to both control ($p < 0.001$) and sham ($p <0.001$) groups (Fig. 6I). This potentiation reflected an increase in the proportion (control = 12%, sham = 12%, mTBI = 56%), but (unlike 1

Hz and 10 Hz continuous stimulation) not the magnitude (post/pre ratio: control = 1.50, sham = 1.23, mTBI = 1.53) of LTP outcomes. There were no effects of 10 Hz discontinuous conditioning on the shape indices of the PSP responses (data not shown).

*3.5 Effect of temporal pattern and treatment condition on plasticity outcome: 100Hz discontinuous conditioning*

For 100 Hz conditioning stimulation, we used only the discontinuous protocol which allowed for rapid recovery of PSP amplitudes during rest intervals [with attendant enduring post tetanic potentiation - see yellow probe trial data during the conditioning period (grey bar) - Figs. 7A-F]. Note that data from the nine stimulation sub-epochs are not shown because most PSPs were embedded in a wave of depolarization and/or had ISIs too short to allow accurate quantification. In control groups, 100 Hz discontinuous perfectly regular (CV 0.0) and slightly irregular (CV 0.2) stimulation produced no net change in average PSP amplitude (*cf.* Figs. 7A-B), while highly irregular stimulation (CV 1.0) induced a net LTD (Fig. 7C) similar to 1 Hz continuous, 10 Hz continuous and 10 Hz discontinuous stimulation (*cf.* Figs. 7C, 4C, 5C, 6C). In contrast, for mTBI groups, perfectly regular stimulation produced net NC (Fig. 7D), slightly irregular stimulation produced a net LTP [(Fig. 7E) which differed from 1 Hz continuous, 10 Hz continuous, and 10 Hz discontinuous stimulation, all of which yielded a net LTD (*cf.* Figs. 7E, 4E, 5E, 6E)], and highly irregular 100 Hz continuous stimulation resulted in net NC [Fig. 7F; which differed from 1 Hz continuous, 10 Hz continuous, and 10 Hz discontinuous stimulation, all of which induced LTP (*cf.* Figs. 4F, 5F, 6F)]. Importantly, despite these modest differences, comparisons between control groups ($p$ = 0.17, Kruskal-Wallis test), or between mTBI groups ($p$ = 0.93, Kruskal-Wallis test) showed no significant effect of temporal pattern on plasticity outcome for the 100 Hz

discontinuous stimulation paradigm. In addition, there was no significant difference in plasticity outcomes between control and mTBI groups for any particular temporal pattern (CV 0.0: $p = 0.40$, MWU test; CV 0.2: $p = 0.97$, MWU test; CV 1.0: $p = 0.28$; *t* test).

Interestingly, for 100 Hz highly irregular stimulation (CV 1.0), the shape indices of PSPs, among the mTBI group show a significant increase in HW (pre: 27 ± 2 ms, post: 30 ± 2 ms, $p = 0.03$; Supp. Fig. 1E) that is non-specific for plasticity outcome (LTD, pre: 30 ± 4 ms, post: 32 ± 4 ms, $p = 0.40$; LTP, pre: 24 ± 3 ms, post: 25 ± 3 ms, $p = 0.26$, paired *t* tests; *cf.* Supp. Figs. 1E-G); while in controls there is no significant change in shape indices overall (DT, pre: 24 ± 2 ms, post: 26 ± 3 ms, $p = 0.54$, paired *t* test; Supp. Fig. 1E), but a significant decrease for those cells responding with LTP (DT, pre: 28 ± 2 ms, post: 25 ± 2 ms, $p = 0.04$; Supp. Fig. 1G) but not LTD (DT, pre: 23 ± 2 ms, post: 26 ± 4 ms, $p = 0.39$; paired *t* tests; Supp. Fig. 1F). In contrast, for 100 Hz slightly irregular (CV = 0.2) stimulation, the mTBI group showed an increase in rise time (RT, pre: 4.7 ± 0.3 ms, post: 6.1 ± 0.5 ms, $p = 0.002$; Supp. Fig. 1H) which was consistent across all plasticity outcomes (LTD, pre: 4.9 ± 0.5 ms, post: 7.1 ± 1.0 ms, $p = 0.035$; LTP, pre: 4.7 ± 0.5 ms, post: 5.6 ± 0.5 ms, $p = 0.006$; paired *t* tests; *cf.* Supp. Fig. 1H-J); while in controls RT was essentially unchanged overall (pre: 5.9 ± 0.6 msec, post: 6.7 ± 0.8 msec, $p = 0.06$) or for any particular plasticity outcome (LTD, pre: 6.1 ± 0.9 msec, post: 7.6 ± 1.8 msec, $p = 0.18$; LTP, pre: 6.5 ± 1.2 msec, post: 6.9 ± 1.0 msec, $p = 0.47$; paired *t* tests; *cf.* Supp. Fig. 1H-J).

*3.6 Kinetic properties of conditioning stimulation responses*

Since we observed a significant difference between control and mTBI group plasticity outcomes only for highly irregular (CV 1.0) 1 Hz continuous, 10 Hz continuous, and 10 Hz discontinuous stimulation we analyzed the kinetic profiles of the conditioning responses for

individual recordings in these groups to determine if they were predictive of plasticity outcome. For 1 Hz continuous highly irregular stimulation we show example time plots of conditioning responses for each treatment group in Fig. 8 (A-C). Notably, the slope of an exponential best fit of normalized conditioning response amplitudes showed a significant positive correlation with plasticity outcomes only in control ($p = 0.02$; Figs. 8A,D) and sham group ($p = 0.048$; Figs. 8B,D), while the slope of a linear best fit shows a significant positive correlation with plasticity outcomes only in the mTBI group ($p = 0.02$, simple linear regression; Figs. 8C,E). The slopes of conditioning response amplitudes did not significantly differ in magnitude for either linear ($p = 0.41$, ANOVA; control = -0.013 ± 0.003, sham = -0.012 ± 0.003, mTBI = -0.007 ± 0.004; data not shown), or exponential ($p = 0.39$ ANOVA; control = -0.019 ± 0.005, sham = -0.018 ± 0.004, mTBI = -0.011 ±0.004; data not shown) best fits. However, relative to control and sham groups, the mTBI group exhibited a significant increase in conditioning amplitude: initial value ($p = 0.002$, Kruskal-Wallis test; with mTBI = 1.19 ± 0.09 vs. control = 0.87 ± 0.05, or sham = 0.90 ± 0.02; $p < 0.001$, $p = 0.003$, Dunn's tests), final value ($p = 0.006$, Kruskal-Wallis test; with mTBI = 1.10 ± 0.12 vs.: control = 0.67 ± 0.04, or sham = 0.72 ± 0.05; $p = 0.001$, $p = 0.007$, Dunn's tests), and average value ($p = 0.01$, Kruskal-Wallis test; with mTBI: 1.15 ± 0.12 vs. control: 0.74 ± 0.04, $p = 0.003$; but not quite for sham: 0.80 ± 0.04; $p = 0.019$ – trend, Dunn's tests; Fig. 8F). Additionally, in the mTBI group, all of these values: average ($p = 0.004$), initial value ($p = 0.007$), and final value ($p = 0.001$, simple linear regression) were predictive of plasticity outcome (Fig. 8G-I); while in the control and sham groups, only the average (control: $p = 0.04$; sham: $p = 0.03$) and final (control: $p = 0.007$; sham: $p = 0.009$; simple linear regression) response amplitudes were predictive of plasticity outcome (Figs. 8G,I).

In contrast, for 10 Hz continuous highly irregular stimulation, the kinetics of the conditioning responses, measured as either slope (Figs. 9A-E) or normalized conditioning response amplitude (Figs. 9G-I) were not predictive of plasticity outcome in any treatment group (control, sham, or mTBI). However, exponential best fits of normalized conditioning amplitude had a significantly more shallow slope in the mTBI group, than in the control or sham groups ($p < 0.001$, ANOVA; with mTBI = -0.580 ± 0.096 vs.: control = -1.045 ± 0.090, or sham = -1.125 ± 0.114; $p = 0.002$, $p < 0.001$, Fisher's LSD tests; data not shown). Moreover, although the conditioning response amplitude was not significantly different between treatment groups initially ($p = 0.15$, Kruskal-Wallis test; with control = 0.786 ± 0.081, sham = 0.693 ± 0.053, mTBI = 0.974 ± 0.110; Fig. 9F), both the average ($p = 0.006$, Kruskal-Wallis test; with mTBI = 0.648 ± 0.093 vs.: control = 0.383 ± 0.035, or sham = 0.360 ± 0.038; $p = 0.009$, $p = 0.002$, Dunn's tests) and final ($p < 0.001$, Kruskal-Wallis test; with mTBI = 0.588 ± 0.091 vs.: control = 0.256 ± 0.022, or sham = 0.234 ± 0.028; $p = 0.0012$, $p < 0.001$, Dunn's tests) amplitudes were significantly higher in the mTBI group than in the control or sham groups (Fig. 9F). Together these data indicate that, during 10 Hz continuous highly irregular conditioning, response amplitudes decreased less and more slowly, in the mTBI group than in the control and sham groups.

For 10 Hz discontinuous highly irregular stimulation, the kinetic profile of the normalized conditioning response amplitudes measured as the average slope of exponential or linear best fits (e.g. Figs. 10A-C), were predictive of plasticity outcome only in the control and sham groups — showing a significant negative correlations for both linear slope (control: $p < 0.001$; sham: $p = 0.02$), and exponential slope (control: $p < 0.001$; sham: $p = 0.04$; simple linear regression; Figs. 10D-E). This result differs from both 1 Hz continuous highly irregular stimulation (significant positive correlation), and 10 Hz continuous highly irregular stimulation (no correlation). Further,

there was no significant difference in the magnitude of conditioning response slopes between control, sham and mTBI groups, for either a: linear (control = -0.560 ± 0.376, sham = -0.908 ± 0.233, mTBI = -1.157 ± 0.155; Kruskal-Wallis test, $p = 0.19$; data not shown) or an exponential best fit (control = -0.899 ± 0.671, sham = -1.555 ± 0.297, mTBI = -1.959 ± 0.388; Kruskal-Wallis test, $p = 0.24$; data not shown). Additionally, there was no significant difference in the magnitude of normalized conditioning response amplitude: average ($p = 0.75$), initial ($p = 0.95$), or final values ($p = 0.41$; Kruskal-Wallis tests; Fig. 10F). However, in the mTBI group, normalized conditioning response amplitude: average ($p = 0.02$), initial value ($p = 0.03$) and final value ($p = 0.02$, simple linear regression) were all predictive of plasticity outcome (significant positive correlation; Figs. 10G-I). In contrast, for the control and sham groups, normalized conditioning response amplitude was not predictive of plasticity outcome for any of these parameters: average (control: $p = 0.71$; sham: $p = 0.35$; Fig. 10G), initial (control: $p = 0.17$; sham: $p = 0.24$; Fig. 10H), or final (control: $p = 0.69$; sham: $p = 0.44$; simple linear regressions; Fig. 10I).

*3.7 Data from our WC recordings appear broadly representative*

In order to assess whether our results from individual cells obtained with WC recordings were reflective of a larger population of synapses in L2/3, we also carried out a series of simultaneous recordings of field potentials (FPs). Representative examples of individual recordings and time plots of WC and FP recordings are shown in Figure 11for: 1 Hz continuous (Figs. 11A-B), 10 Hz continuous (Figs. 11C-D), and 10 Hz discontinuous (Figs. 11E-F) stimulation. Notably, plasticity outcome (measured as a post/pre ratio) was significantly correlated between the simultaneous WC and FP recordings regardless of treatment group: control ($p < 0.001$), sham ($p < 0.001$) or mTBI ($p < 0.001$, simple linear regression; Fig. 11G); or temporal

pattern: CV 0.0 ($p < 0.001$), CV 0.2 ($p < 0.001$) or CV 1.0 ($p < 0.001$, simple linear regression; Fig. 11H). This suggests that our WC data are broadly representative of individual L2/3 pyramidal cell responses over the range of treatment groups and stimulation conditions.

## 4. Discussion

We found that the temporal pattern of conditioning stimulation of synaptic input from layer 4 to layer 2/3 pyramidal neurons in the visual cortex of control rats affects the induction of synaptic plasticity at an intermediate frequency (10 Hz; Figs. 5A-C, 6A-C), where highly irregular stimulation produced LTD, while slightly irregular stimulation resulted in either NC (continuous stimulation) or LTP (discontinuous stimulation), and perfectly regular stimulation produced NC (continuous stimulation) or LTD (discontinuous stimulation). The temporal pattern of conditioning stimulation also played a role in plasticity induction at high frequency (100 Hz; Fig. 7A-C) where a highly irregular stimulation led to LTD, while slightly irregular or perfectly regular stimulation resulted in NC. The temporal pattern of conditioning did not however play a role at low (1 Hz; Fig. 4A-C) frequency where LTD occurred regardless of stimulation regularity.

In contrast, mTBI dramatically affected the dependency of plasticity outcome on the temporal pattern of conditioning. At all frequencies studied (1 Hz, 10 Hz and 100 Hz), with highly irregular temporal patterns of synaptic conditioning stimulation, where cells from controls and shams underwent LTD (Figs. 4C, 5C, 6C, 7C), the neurons from mTBI animals underwent LTP (for 1 Hz or 10 Hz; Figs. 4F, 5F, 6F) or NC (for 100 Hz; Fig. 7F). Moreover, with slightly irregular or perfectly regular temporal patterns of conditioning stimulation, neurons from mTBI animals underwent different plasticity outcomes than those from controls (LTP vs. NC for 10 Hz continuous stimulation, CV 0, *cf.* Figs. 5D, 5A; LTD vs. NC for 10 Hz continuous stimulation, CV

0.2, *cf.* Figs. 5E, 5B; and LTD vs. LTP for 10 Hz discontinuous stimulation, CV 0.2, *cf.* Figs. 6E, 6B). Additionally, for slightly or highly irregular 100 Hz discontinuous stimulation, neurons from mTBI rats displayed different plasticity outcomes from controls (LTP vs. NC for CV 0.2, *cf.* Figs. 7E, 7B; and NC vs. LTD for CV 1.0, *cf.* Figs. 7D, 7A). To our knowledge no previous studies have examined the effect of temporal pattern variation on the induction of LTP or LTD following TBI.

*4.1 Comparison with previous studies on the effects of temporal pattern on synaptic plasticity*

While our findings add new dimensions and have some differences regarding the specific effects of temporal pattern of synaptic conditioning stimulation in brains of normal animals, they are consistent with and build on previous studies that show that temporal pattern is important. For example, studies [119–121] which used a 2 Hz Markovian stimulation with different second order statistics (correlation coefficients of adjacent ISIs) reported that strong negative correlations (-0.8, -0.4) produced LTD, while more positive correlations (0, 0.4, 0.8) produced LTP. Additionally, studies which used a spike timing dependent plasticity paradigm where plasticity was evoked by paired pre-post synaptic stimulation at 0.5–3 Hz, observed LTD if ISIs were regular or had a Gaussian distribution, but no net plasticity (NC) if ISIs had a Poisson distribution [122,123]. It is difficult to make a direct comparison between these studies and our results since we have used a radically different approach in generating our stimulation protocols. However, one study [124] used a similar approach - varying the CV for ISIs - and like them we found that 1 Hz perfectly regular stimulation produced robust LTD, but unlike them we found that 1 Hz highly irregular stimulation often did too. This discrepancy in plasticity outcomes for highly irregular stimulation may reflect subtle but important differences in the temporal pattern of ISIs within the different stimulation protocols in the two studies (although it could also reflect differences in: stimulus pulse

duration, species, pigmentation, or degree of brain maturation including the development of synaptic inhibition).

*4.2 Comparison with previous studies on the effects of TBI on synaptic plasticity*

Our findings in the visual cortex are consistent with previous work in hippocampus indicating that TBI can have an impact on synaptic plasticity. For example, studies of the CA3-CA1 synapse in hippocampus after TBI, have found impairment in the induction and/or maintenance of LTP induced by high frequency regular stimulation [64,125–132], but not LTD induced by low frequency regular stimulation [51,52,59,125,133]. Moreover, several studies (using this same model system) have found that repetitive bursts of high frequency regular stimulation have a greater impact on the induction of LTP after TBI, resulting in either: the abolition of LTP [51,55,134,135], or the induction of LTD [53,136,137].

Like these previous studies, we found that low frequency perfectly regular stimulation (1Hz, 15 min) produced LTD in both control and mTBI animals (*cf.* Figs. 4A,D). Our results for 100 Hz discontinuous regular stimulation (*cf.* Figs. 7A,D) largely recapitulate those of previous studies which used repetitive bursts of high frequency (100 Hz) regular stimulation. Shared features include: 1) an immediate and substantial post-tetanic potentiation which rapidly declines in both control and TBI groups (Figs. 7A,D), 2) no net plasticity (NC) following TBI (Figs. 7D,H), and 3) a greater proportion of LTP responses in the control vs. mTBI group (*cf.* Figs. 7G,H). However, different from our result of net NC in controls, previous studies found a net LTP—but this could reflect a difference in: the number of stimuli [116], number of bursts [138], and/or the duration of interburst intervals [139] during conditioning stimulation.

*4.3 Analyses of PSP shape index and conditioning response kinetics suggest underlying plasticity mechanisms*

Our WC patch clamp experiments recorded the compound PSPs from individual L2/3 pyramidal neurons evoked by stimulation of L4. As such, it is probable that the PSPs included a mixture of excitatory and inhibitory components since inputs to L2/3 pyramidal neurons not only include monosynaptic outputs from L4 excitatory neurons and interlaminar inhibitory projections from L4 but also polysynaptic intralaminar excitatory and inhibitory projections from L2/3 [140–144]. Thus, changes in PSP amplitude after conditioning could potentially reflect an alteration in any of these components. For example, LTD induction of the overall compound PSP could be due to decrease in the strength of excitatory transmission, increased strength of inhibitory transmission or both. Although we did not pharmacologically separate these components in our experiments, we did apply an analysis of shape indices [124,145–148] including the measurement of the evoked PSP half width, rise time and decay time to our WC recordings (Supp. Fig. 1). These results were generally consistent with net LTD of the PSP being due to a decrease in excitatory transmission strength and net LTP being due to an increase in excitatory transmission strength. Moreover, the FP results (Fig. 11G-H) that are generally thought to reflect excitatory synaptic transmission [149,150] were consistent with this result.

Our results show that the frequency, continuity and regularity of synaptic stimulation interact to modify the efficacy of synaptic plasticity, but that interaction of these factors produces different plasticity outcomes in control (naïve) rats and those with mTBI. Applications of these results can also be informed by our results on the utility of the kinetic profile of the synaptic responses during the conditioning (Figs. 8-10) for predicting and achieving the desired plasticity outcome downstream from the stimulation site. Our utilization of probe trials (Figs. 6-7) to assess

synaptic strength throughout the conditioning period is a potentially useful tool for monitoring the kinetics of the change in synaptic strength as it develops so that the stimulation protocols may be adapted in order to achieve the desired plasticity outcome [151–156].

The increased intracellular calcium concentration and input resistance we observed following mTBI (Fig. 2) are indicative of increased neuronal excitability [157,158]. Considerable evidence suggests that differences in the magnitude, duration, rate of rise, source and spatial distribution of intracellular calcium signals are crucial for triggering plasticity in general and LTD vs. LTP in particular [118,153,159–164]. These distinct calcium signals may act differentially on downstream signaling cascades [165–169], activating either kinases or phosphatases, which respectively phosphorylate or dephosphorylate, postsynaptic AMPA receptors [170–175] and translation/transcription factors [176–181]. Moreover, intracellular calcium levels can increase over larger spatial and temporal scales, for example via entry through voltage-gated calcium channels and/or release from intracellular stores [182–186], which can affect processes such as gene expression and protein synthesis that contribute to more persistent synaptic plasticity [187–190].

*4.4 Implications and applications*

One potential application of the findings of our study is to inform design of stimulation parameters for clinical interventions such that different patterns of synaptic stimulation characterized by specific combinations of frequency, continuity and regularity, could be deployed for the appropriate modulation of plasticity outcomes, thereby strengthening or weakening affected neural circuits, in order to promote recovery of cortical function after mTBI. It is encouraging that some studies [191–195] in humans with implanted stimulating electrodes have been shown to have

dramatic results, although the relationship of various stimulation parameters to treatment efficacy are not well understood [196]. Moreover, advances in technology such as the use of low intensity MRI guided transcranial focused ultrasound for neuromodulation [197–199] provide an opportunity to consider such potential therapeutic stimulation protocols without invasive brain surgery for stimulating electrode implantation. However, in order to optimize such approaches, it will be important to select the optimal stimulation patterns and understand the underlying mechanisms to best facilitate any therapeutic gains.

**Acknowledgements**

The authors would like to thank Susanna Kiss for expert technical support for: surgeries, histology, and behavioral experiments.

**Funding**

This work was supported by the Department of Defense (CDMRP grant W81XWH-08-2-0136 to Michael J. Friedlander and the *Mission Connect Mild Traumatic Brain Injury Translational Research Consortium*). The funding source had no involvement in the design of the study; the collection, analysis, or interpretation of the data; or writing of the manuscript.

**Declaration of Competing Interest**

The authors have applied for a patent on the software code (scripts and algorithms) used to generate the temporal patterns of stimulation, as well as the specific temporal patterns, which were used in this study.

## CRediT Authorship Contribution Statement

Conceptualization: QSF, DK, GVDP, PRB, MJF; Methodology: QSF, DK, GVDP, PRB, MJF; Validation: QSF, DK; Formal analysis: QSF, DK, GVDP, CAW; Investigation: QSF, DK, GVDP, CAW; Software: QSF, CAW, PRB; Data curation: QSF, CAW, PRB; Writing – original draft: QSF, MJF; Writing – review and editing: QSF, DK, GVDP, CAW, PRB, MJF; Visualization: QSF, DK, MJF; Supervision: QSF, MJF; Project administration: QSF, MJF; Resources: MJF; Funding Acquisition: MJF. All authors contributed to the manuscript and approved the submitted version.

## References


[1] Gosselin N, Bottari C, Chen J-K, Petrides M, Tinawi S, de Guise E, et al. Electrophysiology and functional MRI in post-acute mild traumatic brain injury. J Neurotrauma 2011;28:329–41. https://doi.org/10.1089/neu.2010.1493.

[2] Petrie EC, Cross DJ, Yarnykh VL, Richards T, Martin NM, Pagulayan K, et al. Neuroimaging, behavioral, and psychological sequelae of repetitive combined blast/impact mild traumatic brain injury in Iraq and Afghanistan war veterans. J Neurotrauma 2014;31:425–36. https://doi.org/10.1089/neu.2013.2952.

[3] Bolouri H, Zetterberg H. Animal Models for Concussion: Molecular and Cognitive Assessments—Relevance to Sport and Military Concussions. In: Kobeissy FH, editor. Brain Neurotrauma: Molecular, Neuropsychological, and Rehabilitation Aspects, Boca Raton (FL): CRC Press/Taylor & Francis; 2015.

[4] Carron SF, Alwis DS, Rajan R. Traumatic Brain Injury and Neuronal Functionality Changes in Sensory Cortex. Front Syst Neurosci 2016;10. https://doi.org/10.3389/fnsys.2016.00047.

[5] Perry DC, Sturm VE, Peterson MJ, Pieper CF, Bullock T, Boeve BF, et al. Association of traumatic brain injury with subsequent neurological and psychiatric disease: a meta-analysis. J Neurosurg 2016;124:511–26. https://doi.org/10.3171/2015.2.JNS14503.

[6] Huang M-X, Huang CW, Harrington DL, Robb-Swan A, Angeles-Quinto A, Nichols S, et al. Resting-state magnetoencephalography source magnitude imaging with deep-learning neural network for classification of symptomatic combat-related mild traumatic brain injury. Hum Brain Mapp 2021;42:1987–2004. https://doi.org/10.1002/hbm.25340.

[7] Hubel DH, Wiesel TN, LeVay S. Plasticity of ocular dominance columns in monkey striate cortex. Philos Trans R Soc Lond B Biol Sci 1977;278:377–409. https://doi.org/10.1098/rstb.1977.0050.

[8] Kim BG, Dai H-N, McAtee M, Vicini S, Bregman BS. Remodeling of synaptic structures in the motor cortex following spinal cord injury. Exp Neurol 2006;198:401–15. https://doi.org/10.1016/j.expneurol.2005.12.010.

[9] Fischer QS, Graves A, Evans S, Lickey ME, Pham TA. Monocular deprivation in adult mice alters visual acuity and single-unit activity. Learn Mem 2007;14:277–86. https://doi.org/10.1101/lm.392107.
[10] Fischer QS, Aleem S, Zhou H, Pham TA. Adult visual experience promotes recovery of primary visual cortex from long-term monocular deprivation. Learn Mem 2007;14:573–80. https://doi.org/10.1101/lm.676707.
[11] Landi D, Rossini PM. Cerebral restorative plasticity from normal ageing to brain diseases: a "never ending story." Restor Neurol Neurosci 2010;28:349–66. https://doi.org/10.3233/RNN-2010-0538.
[12] Raemaekers M, Bergsma DP, van Wezel RJA, van der Wildt GJ, van den Berg AV. Effects of vision restoration training on early visual cortex in patients with cerebral blindness investigated with functional magnetic resonance imaging. J Neurophysiol 2011;105:872–82. https://doi.org/10.1152/jn.00308.2010.
[13] Grasso PA, Gallina J, Bertini C. Shaping the visual system: cortical and subcortical plasticity in the intact and the lesioned brain. Neuropsychologia 2020;142:107464. https://doi.org/10.1016/j.neuropsychologia.2020.107464.
[14] Mowery TM, Garraghty PE. Adult neuroplasticity employs developmental mechanisms. Front Syst Neurosci 2022;16:1086680. https://doi.org/10.3389/fnsys.2022.1086680.
[15] Tsumoto T. Long-term potentiation and long-term depression in the neocortex. Prog Neurobiol 1992;39:209–28. https://doi.org/10.1016/0301-0082(92)90011-3.
[16] Izquierdo I. Pharmacological evidence for a role of long-term potentiation in memory. FASEB J 1994;8:1139–45.
[17] Dan Y, Poo M-M. Spike timing-dependent plasticity of neural circuits. Neuron 2004;44:23–30. https://doi.org/10.1016/j.neuron.2004.09.007.
[18] Malenka RC, Bear MF. LTP and LTD: an embarrassment of riches. Neuron 2004;44:5–21. https://doi.org/10.1016/j.neuron.2004.09.012.
[19] Ge Y, Dong Z, Bagot RC, Howland JG, Phillips AG, Wong TP, et al. Hippocampal long-term depression is required for the consolidation of spatial memory. Proc Natl Acad Sci U S A 2010;107:16697–702. https://doi.org/10.1073/pnas.1008200107.
[20] Madroñal N, Gruart A, Sacktor TC, Delgado-García JM. PKMzeta inhibition reverses learning-induced increases in hippocampal synaptic strength and memory during trace eyeblink conditioning. PLoS One 2010;5:e10400. https://doi.org/10.1371/journal.pone.0010400.
[21] Cooke SF, Bear MF. How the mechanisms of long-term synaptic potentiation and depression serve experience-dependent plasticity in primary visual cortex. Philos Trans R Soc Lond B Biol Sci 2014;369:20130284. https://doi.org/10.1098/rstb.2013.0284.
[22] Nabavi S, Fox R, Proulx CD, Lin JY, Tsien RY, Malinow R. Engineering a memory with LTD and LTP. Nature 2014;511:348–52. https://doi.org/10.1038/nature13294.
[23] Gruart A, Leal-Campanario R, López-Ramos JC, Delgado-García JM. Functional basis of associative learning and its relationships with long-term potentiation evoked in the involved neural circuits: Lessons from studies in behaving mammals. Neurobiol Learn Mem 2015;124:3–18. https://doi.org/10.1016/j.nlm.2015.04.006.
[24] Dringenberg HC. The history of long-term potentiation as a memory mechanism: Controversies, confirmation, and some lessons to remember. Hippocampus 2020;30:987–1012. https://doi.org/10.1002/hipo.23213.
[25] Sánchez-Rodríguez I, Temprano-Carazo S, Jeremic D, Delgado-Garcia JM, Gruart A, Navarro-López JD, et al. Recognition Memory Induces Natural LTP-like Hippocampal Synaptic Excitation and Inhibition. Int J Mol Sci 2022;23:10806. https://doi.org/10.3390/ijms231810806.

[26] Stacho M, Manahan-Vaughan D. The Intriguing Contribution of Hippocampal Long-Term Depression to Spatial Learning and Long-Term Memory. Front Behav Neurosci 2022;16:806356. https://doi.org/10.3389/fnbeh.2022.806356.
[27] Yang X, Gong R, Qin L, Bao Y, Fu Y, Gao S, et al. Trafficking of NMDA receptors is essential for hippocampal synaptic plasticity and memory consolidation. Cell Rep 2022;40:111217. https://doi.org/10.1016/j.celrep.2022.111217.
[28] Bliss TV, Lomo T. Long-lasting potentiation of synaptic transmission in the dentate area of the anaesthetized rabbit following stimulation of the perforant path. J Physiol 1973;232:331–56. https://doi.org/10.1113/jphysiol.1973.sp010273.
[29] Lynch GS, Dunwiddie T, Gribkoff V. Heterosynaptic depression: a postsynaptic correlate of long-term potentiation. Nature 1977;266:737–9. https://doi.org/10.1038/266737a0.
[30] Dudek SM, Bear MF. Homosynaptic long-term depression in area CA1 of hippocampus and effects of N-methyl-D-aspartate receptor blockade. Proc Natl Acad Sci U S A 1992;89:4363–7. https://doi.org/10.1073/pnas.89.10.4363.
[31] Mulkey RM, Malenka RC. Mechanisms underlying induction of homosynaptic long-term depression in area CA1 of the hippocampus. Neuron 1992;9:967–75. https://doi.org/10.1016/0896-6273(92)90248-c.
[32] Artola A, Singer W. Long-term potentiation and NMDA receptors in rat visual cortex. Nature 1987;330:649–52. https://doi.org/10.1038/330649a0.
[33] Kirkwood A, Rioult MC, Bear MF. Experience-dependent modification of synaptic plasticity in visual cortex. Nature 1996;381:526–8. https://doi.org/10.1038/381526a0.
[34] Daw N, Rao Y, Wang X-F, Fischer Q, Yang Y. LTP and LTD vary with layer in rodent visual cortex. Vision Res 2004;44:3377–80. https://doi.org/10.1016/j.visres.2004.09.004.
[35] Lebel D, Grossman Y, Barkai E. Olfactory learning modifies predisposition for long-term potentiation and long-term depression induction in the rat piriform (olfactory) cortex. Cereb Cortex 2001;11:485–9. https://doi.org/10.1093/cercor/11.6.485.
[36] Canto-Bustos M, Friason FK, Bassi C, Oswald A-MM. Disinhibitory Circuitry Gates Associative Synaptic Plasticity in Olfactory Cortex. J Neurosci 2022;42:2942–50. https://doi.org/10.1523/JNEUROSCI.1369-21.2021.
[37] Castro-Alamancos MA, Donoghue JP, Connors BW. Different forms of synaptic plasticity in somatosensory and motor areas of the neocortex. J Neurosci 1995;15:5324–33. https://doi.org/10.1523/JNEUROSCI.15-07-05324.1995.
[38] Froc DJ, Chapman CA, Trepel C, Racine RJ. Long-term depression and depotentiation in the sensorimotor cortex of the freely moving rat. J Neurosci 2000;20:438–45. https://doi.org/10.1523/JNEUROSCI.20-01-00438.2000.
[39] Williams LE, Holtmaat A. Higher-Order Thalamocortical Inputs Gate Synaptic Long-Term Potentiation via Disinhibition. Neuron 2019;101:91-102.e4. https://doi.org/10.1016/j.neuron.2018.10.049.
[40] Calabresi P, Maj R, Pisani A, Mercuri NB, Bernardi G. Long-term synaptic depression in the striatum: physiological and pharmacological characterization. J Neurosci 1992;12:4224–33. https://doi.org/10.1523/JNEUROSCI.12-11-04224.1992.
[41] Calabresi P, Pisani A, Mercuri NB, Bernardi G. Long-term Potentiation in the Striatum is Unmasked by Removing the Voltage-dependent Magnesium Block of NMDA Receptor Channels. Eur J Neurosci 1992;4:929–35. https://doi.org/10.1111/j.1460-9568.1992.tb00119.x.
[42] Crepel F, Jaillard D. Pairing of pre- and postsynaptic activities in cerebellar Purkinje cells induces long-term changes in synaptic efficacy in vitro. J Physiol 1991;432:123–41. https://doi.org/10.1113/jphysiol.1991.sp018380.

[43] Ito M. Cerebellar long-term depression: characterization, signal transduction, and functional roles. Physiol Rev 2001;81:1143–95. https://doi.org/10.1152/physrev.2001.81.3.1143.
[44] Dudek SM, Bear MF. Bidirectional long-term modification of synaptic effectiveness in the adult and immature hippocampus. J Neurosci 1993;13:2910–8. https://doi.org/10.1523/JNEUROSCI.13-07-02910.1993.
[45] Dudek SM, Friedlander MJ. Developmental down-regulation of LTD in cortical layer IV and its independence of modulation by inhibition. Neuron 1996;16:1097–106. https://doi.org/10.1016/s0896-6273(00)80136-1.
[46] Buonomano DV, Merzenich MM. Cortical plasticity: from synapses to maps. Annu Rev Neurosci 1998;21:149–86. https://doi.org/10.1146/annurev.neuro.21.1.149.
[47] Hamdy S, Rothwell JC, Aziz Q, Singh KD, Thompson DG. Long-term reorganization of human motor cortex driven by short-term sensory stimulation. Nat Neurosci 1998;1:64–8. https://doi.org/10.1038/264.
[48] Bach ME, Barad M, Son H, Zhuo M, Lu YF, Shih R, et al. Age-related defects in spatial memory are correlated with defects in the late phase of hippocampal long-term potentiation in vitro and are attenuated by drugs that enhance the cAMP signaling pathway. Proc Natl Acad Sci U S A 1999;96:5280–5. https://doi.org/10.1073/pnas.96.9.5280.
[49] Polley DB, Chen-Bee CH, Frostig RD. Two directions of plasticity in the sensory-deprived adult cortex. Neuron 1999;24:623–37. https://doi.org/10.1016/s0896-6273(00)81117-4.
[50] Kourosh-Arami M, Hosseini N, Komaki A. Brain is modulated by neuronal plasticity during postnatal development. J Physiol Sci 2021;71:34. https://doi.org/10.1186/s12576-021-00819-9.
[51] Schwarzbach E, Bonislawski DP, Xiong G, Cohen AS. Mechanisms underlying the inability to induce area CA1 LTP in the mouse after traumatic brain injury. Hippocampus 2006;16:541–50. https://doi.org/10.1002/hipo.20183.
[52] Albensi BC, Sullivan PG, Thompson MB, Scheff SW, Mattson MP. Cyclosporin ameliorates traumatic brain-injury-induced alterations of hippocampal synaptic plasticity. Exp Neurol 2000;162:385–9. https://doi.org/10.1006/exnr.1999.7338.
[53] Yaka R, Biegon A, Grigoriadis N, Simeonidou C, Grigoriadis S, Alexandrovich AG, et al. D-cycloserine improves functional recovery and reinstates long-term potentiation (LTP) in a mouse model of closed head injury. FASEB J 2007;21:2033–41. https://doi.org/10.1096/fj.06-7856com.
[54] Yamashita S, Hasuo H, Tokutomi T, Shigemori M, Akasu T. Edaravone attenuates impairment of synaptic plasticity in granule cell layer of the dentate gyrus following traumatic brain injury. Kurume Med J 2011;58:47–58. https://doi.org/10.2739/kurumemedj.58.47.
[55] Marshall J, Szmydynger-Chodobska J, Rioult-Pedotti MS, Lau K, Chin AT, Kotla SKR, et al. TrkB-enhancer facilitates functional recovery after traumatic brain injury. Sci Rep 2017;7:10995. https://doi.org/10.1038/s41598-017-11316-8.
[56] Feldmann LK, Le Prieult F, Felzen V, Thal SC, Engelhard K, Behl C, et al. Proteasome and Autophagy-Mediated Impairment of Late Long-Term Potentiation (l-LTP) after Traumatic Brain Injury in the Somatosensory Cortex of Mice. Int J Mol Sci 2019;20:3048. https://doi.org/10.3390/ijms20123048.
[57] Di Lazzaro V, Profice P, Pilato F, Capone F, Ranieri F, Pasqualetti P, et al. Motor cortex plasticity predicts recovery in acute stroke. Cereb Cortex 2010;20:1523–8. https://doi.org/10.1093/cercor/bhp216.
[58] Hosp JA, Luft AR. Dopaminergic meso-cortical projections to m1: role in motor learning and motor cortex plasticity. Front Neurol 2013;4:145. https://doi.org/10.3389/fneur.2013.00145.
[59] Furman JL, Sompol P, Kraner SD, Pleiss MM, Putman EJ, Dunkerson J, et al. Blockade of Astrocytic Calcineurin/NFAT Signaling Helps to Normalize Hippocampal Synaptic Function and Plasticity in a

Rat Model of Traumatic Brain Injury. J Neurosci 2016;36:1502–15. https://doi.org/10.1523/JNEUROSCI.1930-15.2016.
[60] Chou A, Krukowski K, Jopson T, Zhu PJ, Costa-Mattioli M, Walter P, et al. Inhibition of the integrated stress response reverses cognitive deficits after traumatic brain injury. Proc Natl Acad Sci U S A 2017;114:E6420–6. https://doi.org/10.1073/pnas.1707661114.
[61] Chan HH, Wathen CA, Mathews ND, Hogue O, Modic JP, Kundalia R, et al. Lateral cerebellar nucleus stimulation promotes motor recovery and suppresses neuroinflammation in a fluid percussion injury rodent model. Brain Stimul 2018;11:1356–67. https://doi.org/10.1016/j.brs.2018.07.051.
[62] Shin SS, Krishnan V, Stokes W, Robertson C, Celnik P, Chen Y, et al. Transcranial magnetic stimulation and environmental enrichment enhances cortical excitability and functional outcomes after traumatic brain injury. Brain Stimulation 2018;11:1306–13. https://doi.org/10.1016/j.brs.2018.07.050.
[63] Nagao S, Ito M. Roles of Synaptic Plasticity in Functional Recovery After Brain Injury. In: Petrosini L, editor. Neurobiological and Psychological Aspects of Brain Recovery, Cham: Springer International Publishing; 2023, p. 177–207. https://doi.org/10.1007/978-3-031-24930-3_8.
[64] Zhang B, Chen X, Lin Y, Tan T, Yang Z, Dayao C, et al. Impairment of synaptic plasticity in hippocampus is exacerbated by methylprednisolone in a rat model of traumatic brain injury. Brain Res 2011;1382:165–72. https://doi.org/10.1016/j.brainres.2011.01.065.
[65] De Beaumont L, Tremblay S, Poirier J, Lassonde M, Théoret H. Altered bidirectional plasticity and reduced implicit motor learning in concussed athletes. Cereb Cortex 2012;22:112–21. https://doi.org/10.1093/cercor/bhr096.
[66] Dorsett CR, McGuire JL, DePasquale EAK, Gardner AE, Floyd CL, McCullumsmith RE. Glutamate Neurotransmission in Rodent Models of Traumatic Brain Injury. J Neurotrauma 2017;34:263–72. https://doi.org/10.1089/neu.2015.4373.
[67] Breit S, Schulz JB, Benabid A-L. Deep brain stimulation. Cell Tissue Res 2004;318:275–88. https://doi.org/10.1007/s00441-004-0936-0.
[68] Krauss JK, Lipsman N, Aziz T, Boutet A, Brown P, Chang JW, et al. Technology of deep brain stimulation: current status and future directions. Nat Rev Neurol 2021;17:75–87. https://doi.org/10.1038/s41582-020-00426-z.
[69] Baek H, Pahk KJ, Kim H. A review of low-intensity focused ultrasound for neuromodulation. Biomed Eng Lett 2017;7:135–42. https://doi.org/10.1007/s13534-016-0007-y.
[70] di Biase L, Falato E, Di Lazzaro V. Transcranial Focused Ultrasound (tFUS) and Transcranial Unfocused Ultrasound (tUS) Neuromodulation: From Theoretical Principles to Stimulation Practices. Front Neurol 2019;10:549. https://doi.org/10.3389/fneur.2019.00549.
[71] Hallett M. Transcranial magnetic stimulation: a primer. Neuron 2007;55:187–99. https://doi.org/10.1016/j.neuron.2007.06.026.
[72] Wassermann EM, Zimmermann T. Transcranial magnetic brain stimulation: therapeutic promises and scientific gaps. Pharmacol Ther 2012;133:98–107. https://doi.org/10.1016/j.pharmthera.2011.09.003.
[73] Ranieri F, Coppola G, Musumeci G, Capone F, Di Pino G, Parisi V, et al. Evidence for associative plasticity in the human visual cortex. Brain Stimul 2019;12:705–13. https://doi.org/10.1016/j.brs.2019.01.021.
[74] Nitsche MA, Paulus W. Excitability changes induced in the human motor cortex by weak transcranial direct current stimulation. J Physiol 2000;527 Pt 3:633–9. https://doi.org/10.1111/j.1469-7793.2000.t01-1-00633.x.
[75] Quinn DK, Story-Remer J, Brandt E, Fratzke V, Rieger R, Wilson JK, et al. Transcranial direct current stimulation modulates working memory and prefrontal-insula connectivity after mild-

moderate traumatic brain injury. Front Hum Neurosci 2022;16:1026639. https://doi.org/10.3389/fnhum.2022.1026639.
[76] Liu X, Qiu F, Hou L, Wang X. Review of Noninvasive or Minimally Invasive Deep Brain Stimulation. Front Behav Neurosci 2021;15:820017. https://doi.org/10.3389/fnbeh.2021.820017.
[77] Benabid AL, Pollak P, Gross C, Hoffmann D, Benazzouz A, Gao DM, et al. Acute and long-term effects of subthalamic nucleus stimulation in Parkinson's disease. Stereotact Funct Neurosurg 1994;62:76–84. https://doi.org/10.1159/000098600.
[78] Chung CL-H, Mak MK-Y, Hallett M. Transcranial Magnetic Stimulation Promotes Gait Training in Parkinson Disease. Ann Neurol 2020;88:933–45. https://doi.org/10.1002/ana.25881.
[79] Liu X, Liu H, Liu Z, Rao J, Wang J, Wang P, et al. Transcranial Direct Current Stimulation for Parkinson's Disease: A Systematic Review and Meta-Analysis. Front Aging Neurosci 2021;13:746797. https://doi.org/10.3389/fnagi.2021.746797.
[80] Jeong H, Im JJ, Park J-S, Na S-H, Lee W, Yoo S-S, et al. A pilot clinical study of low-intensity transcranial focused ultrasound in Alzheimer's disease. Ultrasonography 2021;40:512–9. https://doi.org/10.14366/usg.20138.
[81] Luo Y, Sun Y, Tian X, Zheng X, Wang X, Li W, et al. Deep Brain Stimulation for Alzheimer's Disease: Stimulation Parameters and Potential Mechanisms of Action. Front Aging Neurosci 2021;13:619543. https://doi.org/10.3389/fnagi.2021.619543.
[82] Wu C, Yang L, Feng S, Zhu L, Yang L, Liu TC-Y, et al. Therapeutic non-invasive brain treatments in Alzheimer's disease: recent advances and challenges. Inflamm Regen 2022;42:31. https://doi.org/10.1186/s41232-022-00216-8.
[83] Elder C, Friedman D, Devinsky O, Doyle W, Dugan P. Responsive neurostimulation targeting the anterior nucleus of the thalamus in 3 patients with treatment-resistant multifocal epilepsy. Epilepsia Open 2019;4:187–92. https://doi.org/10.1002/epi4.12300.
[84] Tsuboyama M, Kaye HL, Rotenberg A. Review of Transcranial Magnetic Stimulation in Epilepsy. Clin Ther 2020;42:1155–68. https://doi.org/10.1016/j.clinthera.2020.05.016.
[85] Sudbrack-Oliveira P, Barbosa MZ, Thome-Souza S, Razza LB, Gallucci-Neto J, da Costa Lane Valiengo L, et al. Transcranial direct current stimulation (tDCS) in the management of epilepsy: A systematic review. Seizure 2021;86:85–95. https://doi.org/10.1016/j.seizure.2021.01.020.
[86] Mayberg HS, Lozano AM, Voon V, McNeely HE, Seminowicz D, Hamani C, et al. Deep brain stimulation for treatment-resistant depression. Neuron 2005;45:651–60. https://doi.org/10.1016/j.neuron.2005.02.014.
[87] Perera T, George MS, Grammer G, Janicak PG, Pascual-Leone A, Wirecki TS. The Clinical TMS Society Consensus Review and Treatment Recommendations for TMS Therapy for Major Depressive Disorder. Brain Stimul 2016;9:336–46. https://doi.org/10.1016/j.brs.2016.03.010.
[88] Jog MV, Wang DJJ, Narr KL. A review of transcranial direct current stimulation (tDCS) for the individualized treatment of depressive symptoms. Pers Med Psychiatry 2019;17–18:17–22. https://doi.org/10.1016/j.pmip.2019.03.001.
[89] Alagapan S, Choi KS, Heisig S, Riva-Posse P, Crowell A, Tiruvadi V, et al. Cingulate dynamics track depression recovery with deep brain stimulation. Nature 2023. https://doi.org/10.1038/s41586-023-06541-3.
[90] Brocker DT, Swan BD, So RQ, Turner DA, Gross RE, Grill WM. Optimized temporal pattern of brain stimulation designed by computational evolution. Sci Transl Med 2017;9:eaah3532. https://doi.org/10.1126/scitranslmed.aah3532.
[91] Cagnan H, Denison T, McIntyre C, Brown P. Emerging technologies for improved deep brain stimulation. Nat Biotechnol 2019;37:1024–33. https://doi.org/10.1038/s41587-019-0244-6.

[92] Okun MS, Hickey PT, Machado AG, Kuncel AM, Grill WM. Temporally optimized patterned stimulation (TOPS®) as a therapy to personalize deep brain stimulation treatment of Parkinson's disease. Front Hum Neurosci 2022;16:929509. https://doi.org/10.3389/fnhum.2022.929509.
[93] Collingridge GL, Kehl SJ, McLennan H. Excitatory amino acids in synaptic transmission in the Schaffer collateral-commissural pathway of the rat hippocampus. J Physiol 1983;334:33–46. https://doi.org/10.1113/jphysiol.1983.sp014478.
[94] Bear MF, Kirkwood A. Neocortical long-term potentiation. Curr Opin Neurobiol 1993;3:197–202. https://doi.org/10.1016/0959-4388(93)90210-p.
[95] Kirkwood A, Bear MF. Homosynaptic long-term depression in the visual cortex. J Neurosci 1994;14:3404–12. https://doi.org/10.1523/JNEUROSCI.14-05-03404.1994.
[96] Levy WB, Steward O. Temporal contiguity requirements for long-term associative potentiation/depression in the hippocampus. Neuroscience 1983;8:791–7. https://doi.org/10.1016/0306-4522(83)90010-6.
[97] Frégnac Y, Burke JP, Smith D, Friedlander MJ. Temporal covariance of pre- and postsynaptic activity regulates functional connectivity in the visual cortex. J Neurophysiol 1994;71:1403–21. https://doi.org/10.1152/jn.1994.71.4.1403.
[98] Huang S, Rozas C, Treviño M, Contreras J, Yang S, Song L, et al. Associative Hebbian synaptic plasticity in primate visual cortex. J Neurosci 2014;34:7575–9. https://doi.org/10.1523/JNEUROSCI.0983-14.2014.
[99] Baker MA. Spontaneous and evoked activity of neurones in the somatosensory thalamus of the waking cat. J Physiol 1971;217:359–79. https://doi.org/10.1113/jphysiol.1971.sp009576.
[100] Rowe MH, Fischer Q. Dynamic properties of retino-geniculate synapses in the cat. Vis Neurosci 2001;18:219–31. https://doi.org/10.1017/s0952523801182076.
[101] Swadlow HA, Bezdudnaya T, Gusev AG. Spike timing and synaptic dynamics at the awake thalamocortical synapse. Prog Brain Res 2005;149:91–105. https://doi.org/10.1016/S0079-6123(05)49008-1.
[102] Luczak A, Barthó P, Marguet SL, Buzsáki G, Harris KD. Sequential structure of neocortical spontaneous activity in vivo. Proc Natl Acad Sci U S A 2007;104:347–52. https://doi.org/10.1073/pnas.0605643104.
[103] Boyer M, Baudin P, Stengel C, Valero-Cabré A, Lohof AM, Charpier S, et al. In vivo low-intensity magnetic pulses durably alter neocortical neuron excitability and spontaneous activity. J Physiol 2022;600:4019–37. https://doi.org/10.1113/JP283244.
[104] Armstrong DM, Rawson JA. Activity patterns of cerebellar cortical neurones and climbing fibre afferents in the awake cat. J Physiol 1979;289:425–48. https://doi.org/10.1113/jphysiol.1979.sp012745.
[105] Softky WR, Koch C. The highly irregular firing of cortical cells is inconsistent with temporal integration of random EPSPs. J Neurosci 1993;13:334–50. https://doi.org/10.1523/JNEUROSCI.13-01-00334.1993.
[106] Shadlen MN, Newsome WT. The variable discharge of cortical neurons: implications for connectivity, computation, and information coding. J Neurosci 1998;18:3870–96. https://doi.org/10.1523/JNEUROSCI.18-10-03870.1998.
[107] Stevens CF, Zador AM. Input synchrony and the irregular firing of cortical neurons. Nat Neurosci 1998;1:210–7. https://doi.org/10.1038/659.
[108] Sabatier N, Leng G. Spontaneous discharge characteristic of neurons in the ventromedial nucleus of the rat hypothalamus in vivo. Eur J Neurosci 2008;28:693–706. https://doi.org/10.1111/j.1460-9568.2008.06389.x.

[109] Festa D, Aschner A, Davila A, Kohn A, Coen-Cagli R. Neuronal variability reflects probabilistic inference tuned to natural image statistics. Nat Commun 2021;12:3635. https://doi.org/10.1038/s41467-021-23838-x.
[110] Cherian L, Robertson CS, Contant CF, Bryan RM. Lateral cortical impact injury in rats: cerebrovascular effects of varying depth of cortical deformation and impact velocity. J Neurotrauma 1994;11:573–85. https://doi.org/10.1089/neu.1994.11.573.
[111] Cherian L, Robertson CS, Goodman JC. Secondary insults increase injury after controlled cortical impact in rats. J Neurotrauma 1996;13:371–83. https://doi.org/10.1089/neu.1996.13.371.
[112] Navarro JC, Pillai S, Cherian L, Garcia R, Grill RJ, Robertson CS. Histopathological and behavioral effects of immediate and delayed hemorrhagic shock after mild traumatic brain injury in rats. J Neurotrauma 2012;29:322–34. https://doi.org/10.1089/neu.2011.1979.
[113] McCormick DA, Connors BW, Lighthall JW, Prince DA. Comparative electrophysiology of pyramidal and sparsely spiny stellate neurons of the neocortex. J Neurophysiol 1985;54:782–806. https://doi.org/10.1152/jn.1985.54.4.782.
[114] Connors BW, Gutnick MJ. Intrinsic firing patterns of diverse neocortical neurons. Trends Neurosci 1990;13:99–104. https://doi.org/10.1016/0166-2236(90)90185-d.
[115] Varela JA, Song S, Turrigiano GG, Nelson SB. Differential depression at excitatory and inhibitory synapses in visual cortex. J Neurosci 1999;19:4293–304. https://doi.org/10.1523/JNEUROSCI.19-11-04293.1999.
[116] Kim E, Owen B, Holmes WR, Grover LM. Decreased afferent excitability contributes to synaptic depression during high-frequency stimulation in hippocampal area CA1. J Neurophysiol 2012;108:1965–76. https://doi.org/10.1152/jn.00276.2011.
[117] Sørensen JB, Matti U, Wei S-H, Nehring RB, Voets T, Ashery U, et al. The SNARE protein SNAP-25 is linked to fast calcium triggering of exocytosis. Proc Natl Acad Sci U S A 2002;99:1627–32. https://doi.org/10.1073/pnas.251673298.
[118] Ismailov I, Kalikulov D, Inoue T, Friedlander MJ. The kinetic profile of intracellular calcium predicts long-term potentiation and long-term depression. J Neurosci 2004;24:9847–61. https://doi.org/10.1523/JNEUROSCI.0738-04.2004.
[119] Tsukada M, Aihara T, Mizuno M, Kato H, Ito K. Temporal pattern sensitivity of long-term potentiation in hippocampal CA1 neurons. Biol Cybern 1994;70:495–503. https://doi.org/10.1007/BF00198802.
[120] Tsukada M, Ichinose N, Aihara K, Ito H, Fujii H. Dynamical Cell Assembly Hypothesis - Theoretical Possibility of Spatio-temporal Coding in the Cortex. Neural Netw 1996;9:1303–50.
[121] Aihara T, Kobayashi Y, Tsukada M. Spatiotemporal visualization of long-term potentiation and depression in the hippocampal CA1 area. Hippocampus 2005;15:68–78. https://doi.org/10.1002/hipo.20031.
[122] Guo Y, Huang S, de Pasquale R, McGehrin K, Lee H-K, Zhao K, et al. Dark exposure extends the integration window for spike-timing-dependent plasticity. J Neurosci 2012;32:15027–35. https://doi.org/10.1523/JNEUROSCI.2545-12.2012.
[123] Cui Y, Prokin I, Mendes A, Berry H, Venance L. Robustness of STDP to spike timing jitter. Sci Rep 2018;8:8139. https://doi.org/10.1038/s41598-018-26436-y.
[124] Perrett SP, Dudek SM, Eagleman D, Montague PR, Friedlander MJ. LTD induction in adult visual cortex: role of stimulus timing and inhibition. J Neurosci 2001;21:2308–19. https://doi.org/10.1523/JNEUROSCI.21-07-02308.2001.
[125] D'Ambrosio R, Maris DO, Grady MS, Winn HR, Janigro D. Selective loss of hippocampal long-term potentiation, but not depression, following fluid percussion injury. Brain Res 1998;786:64–79. https://doi.org/10.1016/s0006-8993(97)01412-1.

[126] Sanders MJ, Sick TJ, Perez-Pinzon MA, Dietrich WD, Green EJ. Chronic failure in the maintenance of long-term potentiation following fluid percussion injury in the rat. Brain Res 2000;861:69–76. https://doi.org/10.1016/s0006-8993(00)01986-7.
[127] Norris CM, Scheff SW. Recovery of afferent function and synaptic strength in hippocampal CA1 following traumatic brain injury. J Neurotrauma 2009;26:2269–78. https://doi.org/10.1089/neu.2009.1029.
[128] Titus DJ, Furones C, Kang Y, Atkins CM. Age-dependent alterations in cAMP signaling contribute to synaptic plasticity deficits following traumatic brain injury. Neuroscience 2013;231:182–94. https://doi.org/10.1016/j.neuroscience.2012.12.002.
[129] Corser-Jensen CE, Goodell DJ, Freund RK, Serbedzija P, Murphy RC, Farias SE, et al. Blocking leukotriene synthesis attenuates the pathophysiology of traumatic brain injury and associated cognitive deficits. Exp Neurol 2014;256:7–16. https://doi.org/10.1016/j.expneurol.2014.03.008.
[130] White ER, Pinar C, Bostrom CA, Meconi A, Christie BR. Mild Traumatic Brain Injury Produces Long-Lasting Deficits in Synaptic Plasticity in the Female Juvenile Hippocampus. Journal of Neurotrauma 2017;34:1111–23. https://doi.org/10.1089/neu.2016.4638.
[131] Franklin W, Krishnan B, Taglialatela G. Chronic synaptic insulin resistance after traumatic brain injury abolishes insulin protection from amyloid beta and tau oligomer-induced synaptic dysfunction. Sci Rep 2019;9:8228. https://doi.org/10.1038/s41598-019-44635-z.
[132] Lecca D, Bader M, Tweedie D, Hoffman AF, Jung YJ, Hsueh S-C, et al. (-)-Phenserine and the prevention of pre-programmed cell death and neuroinflammation in mild traumatic brain injury and Alzheimer's disease challenged mice. Neurobiol Dis 2019;130:104528. https://doi.org/10.1016/j.nbd.2019.104528.
[133] Norris CM, Sompol P, Roberts KN, Ansari M, Scheff SW. Pycnogenol protects CA3-CA1 synaptic function in a rat model of traumatic brain injury. Exp Neurol 2016;276:5–12. https://doi.org/10.1016/j.expneurol.2015.11.006.
[134] Perez EJ, Tapanes SA, Loris ZB, Balu DT, Sick TJ, Coyle JT, et al. Enhanced astrocytic d-serine underlies synaptic damage after traumatic brain injury. J Clin Invest 2017;127:3114–25. https://doi.org/10.1172/JCI92300.
[135] Wang W, Zhang X, He R, Li S, Fang D, Pang C. Gamma frequency entrainment rescues cognitive impairment by decreasing postsynaptic transmission after traumatic brain injury. CNS Neurosci Ther 2023;29:1142–53. https://doi.org/10.1111/cns.14096.
[136] Reeves TM, Lyeth BG, Povlishock JT. Long-term potentiation deficits and excitability changes following traumatic brain injury. Exp Brain Res 1995;106:248–56. https://doi.org/10.1007/BF00241120.
[137] Perez EJ, Cepero ML, Perez SU, Coyle JT, Sick TJ, Liebl DJ. EphB3 signaling propagates synaptic dysfunction in the traumatic injured brain. Neurobiol Dis 2016;94:73–84. https://doi.org/10.1016/j.nbd.2016.06.007.
[138] Hernandez RV, Navarro MM, Rodriguez WA, Martinez JL, LeBaron RG. Differences in the magnitude of long-term potentiation produced by theta burst and high frequency stimulation protocols matched in stimulus number. Brain Res Brain Res Protoc 2005;15:6–13. https://doi.org/10.1016/j.brainresprot.2005.02.003.
[139] Grover LM, Kim E, Cooke JD, Holmes WR. LTP in hippocampal area CA1 is induced by burst stimulation over a broad frequency range centered around delta. Learn Mem 2009;16:69–81. https://doi.org/10.1101/lm.1179109.
[140] Douglas RJ, Martin KAC. NEURONAL CIRCUITS OF THE NEOCORTEX. Annu Rev Neurosci 2004;27:419–51. https://doi.org/10.1146/annurev.neuro.27.070203.144152.
[141] Brown SP, Hestrin S. Cell-type identity: a key to unlocking the function of neocortical circuits. Curr Opin Neurobiol 2009;19:415–21. https://doi.org/10.1016/j.conb.2009.07.011.

[142] Hang GB, Dan Y. Asymmetric temporal integration of layer 4 and layer 2/3 inputs in visual cortex. J Neurophysiol 2011;105:347–55. https://doi.org/10.1152/jn.00159.2010.
[143] Xu X, Olivas ND, Ikrar T, Peng T, Holmes TC, Nie Q, et al. Primary visual cortex shows laminar-specific and balanced circuit organization of excitatory and inhibitory synaptic connectivity. J Physiol 2016;594:1891–910. https://doi.org/10.1113/JP271891.
[144] Schneider-Mizell CM, Bodor A, Brittain D, Buchanan J, Bumbarger DJ, Elabbady L, et al. Cell-type-specific inhibitory circuitry from a connectomic census of mouse visual cortex. Neuroscience; 2023. https://doi.org/10.1101/2023.01.23.525290.
[145] Jack JJ, Redman SJ. An electrical description of the motoneurone, and its application to the analysis of synaptic potentials. J Physiol 1971;215:321–52. https://doi.org/10.1113/jphysiol.1971.sp009473.
[146] Jack JJ, Miller S, Porter R, Redman SJ. The time course of minimal excitory post-synaptic potentials evoked in spinal motoneurones by group Ia afferent fibres. J Physiol 1971;215:353–80. https://doi.org/10.1113/jphysiol.1971.sp009474.
[147] Turner DA. Feed-forward inhibitory potentials and excitatory interactions in guinea-pig hippocampal pyramidal cells. J Physiol 1990;422:333–50. https://doi.org/10.1113/jphysiol.1990.sp017987.
[148] Yarden-Rabinowitz Y, Yarom Y. In vivo analysis of synaptic activity in cerebellar nuclei neurons unravels the efficacy of excitatory inputs. J Physiol 2017;595:5945–63. https://doi.org/10.1113/JP274115.
[149] Mitzdorf U, Singer W. Prominent excitatory pathways in the cat visual cortex (A 17 and A 18): a current source density analysis of electrically evoked potentials. Exp Brain Res 1978;33:371–94. https://doi.org/10.1007/BF00235560.
[150] Haider B, Schulz DPA, Häusser M, Carandini M. Millisecond Coupling of Local Field Potentials to Synaptic Currents in the Awake Visual Cortex. Neuron 2016;90:35–42. https://doi.org/10.1016/j.neuron.2016.02.034.
[151] Katz B, Miledi R. The role of calcium in neuromuscular facilitation. J Physiol 1968;195:481–92. https://doi.org/10.1113/jphysiol.1968.sp008469.
[152] Stevens CF, Tonegawa S, Wang Y. The role of calcium-calmodulin kinase II in three forms of synaptic plasticity. Curr Biol 1994;4:687–93. https://doi.org/10.1016/s0960-9822(00)00153-6.
[153] Zucker RS. Calcium- and activity-dependent synaptic plasticity. Curr Opin Neurobiol 1999;9:305–13. https://doi.org/10.1016/s0959-4388(99)80045-2.
[154] Seki K, Kudoh M, Shibuki K. Sequence dependence of post-tetanic potentiation after sequential heterosynaptic stimulation in the rat auditory cortex. J Physiol 2001;533:503–18. https://doi.org/10.1111/j.1469-7793.2001.0503a.x.
[155] Kitaura H, Hishida R, Kudoh M, Shibuki K. Activity-dependent persisting modification of polysynaptic neural circuits involving layer V pyramidal neurons in rat auditory cortex in vitro. Eur J Neurosci 2004;19:356–64. https://doi.org/10.1111/j.0953-816x.2003.03136.x.
[156] Hughes C, Kozai T. Dynamic amplitude modulation of microstimulation evokes biomimetic onset and offset transients and reduces depression of evoked calcium responses in sensory cortices. Brain Stimul 2023;16:939–65. https://doi.org/10.1016/j.brs.2023.05.013.
[157] Kaufmann TJ, Harrison PM, Richardson MJE, Pinheiro TJT, Wall MJ. Intracellular soluble α-synuclein oligomers reduce pyramidal cell excitability. J Physiol 2016;594:2751–72. https://doi.org/10.1113/JP271968.
[158] Sun J, Jacobs KM. Knockout of Cyclophilin-D Provides Partial Amelioration of Intrinsic and Synaptic Properties Altered by Mild Traumatic Brain Injury. Front Syst Neurosci 2016;10:63. https://doi.org/10.3389/fnsys.2016.00063.

[159] Artola A, Singer W. Long-term depression of excitatory synaptic transmission and its relationship to long-term potentiation. Trends Neurosci 1993;16:480–7. https://doi.org/10.1016/0166-2236(93)90081-v.
[160] Kato N, Tanaka T, Yamamoto K, Isomura Y. Distinct temporal profiles of activity-dependent calcium increase in pyramidal neurons of the rat visual cortex. J Physiol 1999;519 Pt 2:467–79. https://doi.org/10.1111/j.1469-7793.1999.0467m.x.
[161] Yang SN, Tang YG, Zucker RS. Selective induction of LTP and LTD by postsynaptic [Ca2+]i elevation. J Neurophysiol 1999;81:781–7. https://doi.org/10.1152/jn.1999.81.2.781.
[162] Evans RC, Blackwell KT. Calcium: amplitude, duration, or location? Biol Bull 2015;228:75–83. https://doi.org/10.1086/BBLv228n1p75.
[163] Ebner C, Clopath C, Jedlicka P, Cuntz H. Unifying Long-Term Plasticity Rules for Excitatory Synapses by Modeling Dendrites of Cortical Pyramidal Neurons. Cell Rep 2019;29:4295-4307.e6. https://doi.org/10.1016/j.celrep.2019.11.068.
[164] Landau AT, Park P, Wong-Campos JD, Tian H, Cohen AE, Sabatini BL. Dendritic branch structure compartmentalizes voltage-dependent calcium influx in cortical layer 2/3 pyramidal cells. Elife 2022;11:e76993. https://doi.org/10.7554/eLife.76993.
[165] Lisman JE. Three Ca2+ levels affect plasticity differently: the LTP zone, the LTD zone and no man's land. J Physiol 2001;532:285. https://doi.org/10.1111/j.1469-7793.2001.0285f.x.
[166] Kennedy MB. Synaptic Signaling in Learning and Memory. Cold Spring Harb Perspect Biol 2013;8:a016824. https://doi.org/10.1101/cshperspect.a016824.
[167] Baudry M, Zhu G, Liu Y, Wang Y, Briz V, Bi X. Multiple cellular cascades participate in long-term potentiation and in hippocampus-dependent learning. Brain Res 2015;1621:73–81. https://doi.org/10.1016/j.brainres.2014.11.033.
[168] Hidalgo C, Arias-Cavieres A. Calcium, Reactive Oxygen Species, and Synaptic Plasticity. Physiology (Bethesda) 2016;31:201–15. https://doi.org/10.1152/physiol.00038.2015.
[169] Yasuda R. Biophysics of Biochemical Signaling in Dendritic Spines: Implications in Synaptic Plasticity. Biophys J 2017;113:2152–9. https://doi.org/10.1016/j.bpj.2017.07.029.
[170] Lisman J. A mechanism for the Hebb and the anti-Hebb processes underlying learning and memory. Proc Natl Acad Sci U S A 1989;86:9574–8. https://doi.org/10.1073/pnas.86.23.9574.
[171] Lee HK, Barbarosie M, Kameyama K, Bear MF, Huganir RL. Regulation of distinct AMPA receptor phosphorylation sites during bidirectional synaptic plasticity. Nature 2000;405:955–9. https://doi.org/10.1038/35016089.
[172] Smolen P, Baxter DA, Byrne JH. A model of the roles of essential kinases in the induction and expression of late long-term potentiation. Biophys J 2006;90:2760–75. https://doi.org/10.1529/biophysj.105.072470.
[173] Kubota Y, Waxham MN. Lobe specific Ca2+-calmodulin nano-domain in neuronal spines: a single molecule level analysis. PLoS Comput Biol 2010;6:e1000987. https://doi.org/10.1371/journal.pcbi.1000987.
[174] Woolfrey KM, Dell'Acqua ML. Coordination of Protein Phosphorylation and Dephosphorylation in Synaptic Plasticity. J Biol Chem 2015;290:28604–12. https://doi.org/10.1074/jbc.R115.657262.
[175] Bayer KU, Schulman H. CaM Kinase: Still Inspiring at 40. Neuron 2019;103:380–94. https://doi.org/10.1016/j.neuron.2019.05.033.
[176] Atkins CM, Davare MA, Oh MC, Derkach V, Soderling TR. Bidirectional regulation of cytoplasmic polyadenylation element-binding protein phosphorylation by Ca2+/calmodulin-dependent protein kinase II and protein phosphatase 1 during hippocampal long-term potentiation. J Neurosci 2005;25:5604–10. https://doi.org/10.1523/JNEUROSCI.5051-04.2005.
[177] Mauna JC, Miyamae T, Pulli B, Thiels E. Protein phosphatases 1 and 2A are both required for long-term depression and associated dephosphorylation of cAMP response element binding protein in

hippocampal area CA1 in vivo. Hippocampus 2011;21:1093–104. https://doi.org/10.1002/hipo.20823.
[178] Dong C, Vashisht A, Hegde AN. Proteasome regulates the mediators of cytoplasmic polyadenylation signaling during late-phase long-term potentiation. Neurosci Lett 2014;583:199–204. https://doi.org/10.1016/j.neulet.2014.09.038.
[179] Ma H, Li B, Tsien RW. Distinct roles of multiple isoforms of CaMKII in signaling to the nucleus. Biochim Biophys Acta 2015;1853:1953–7. https://doi.org/10.1016/j.bbamcr.2015.02.008.
[180] Shioda N, Fukunaga K. Physiological and Pathological Roles of CaMKII-PP1 Signaling in the Brain. Int J Mol Sci 2017;19:20. https://doi.org/10.3390/ijms19010020.
[181] Laviv T, Scholl B, Parra-Bueno P, Foote B, Zhang C, Yan L, et al. In Vivo Imaging of the Coupling between Neuronal and CREB Activity in the Mouse Brain. Neuron 2020;105:799-812.e5. https://doi.org/10.1016/j.neuron.2019.11.028.
[182] Jaffe DB, Brown TH. Metabotropic glutamate receptor activation induces calcium waves within hippocampal dendrites. J Neurophysiol 1994;72:471–4. https://doi.org/10.1152/jn.1994.72.1.471.
[183] Nishiyama M, Hong K, Mikoshiba K, Poo MM, Kato K. Calcium stores regulate the polarity and input specificity of synaptic modification. Nature 2000;408:584–8. https://doi.org/10.1038/35046067.
[184] Zufall F, Leinders-Zufall T, Greer CA. Amplification of odor-induced Ca(2+) transients by store-operated Ca(2+) release and its role in olfactory signal transduction. J Neurophysiol 2000;83:501–12. https://doi.org/10.1152/jn.2000.83.1.501.
[185] Matamales M. Neuronal activity-regulated gene transcription: how are distant synaptic signals conveyed to the nucleus? F1000Res 2012;1:69. https://doi.org/10.12688/f1000research.1-69.v1.
[186] Ashhad S, Narayanan R. Stores, Channels, Glue, and Trees: Active Glial and Active Dendritic Physiology. Mol Neurobiol 2019;56:2278–99. https://doi.org/10.1007/s12035-018-1223-5.
[187] West AE, Chen WG, Dalva MB, Dolmetsch RE, Kornhauser JM, Shaywitz AJ, et al. Calcium regulation of neuronal gene expression. Proc Natl Acad Sci U S A 2001;98:11024–31. https://doi.org/10.1073/pnas.191352298.
[188] Chen WG, West AE, Tao X, Corfas G, Szentirmay MN, Sawadogo M, et al. Upstream stimulatory factors are mediators of Ca2+-responsive transcription in neurons. J Neurosci 2003;23:2572–81. https://doi.org/10.1523/JNEUROSCI.23-07-02572.2003.
[189] Tabuchi A. Synaptic plasticity-regulated gene expression: a key event in the long-lasting changes of neuronal function. Biol Pharm Bull 2008;31:327–35. https://doi.org/10.1248/bpb.31.327.
[190] Karpova A, Samer S, Turacak R, Yuanxiang P, Kreutz MR. Integration of nuclear Ca2+ transients and subnuclear protein shuttling provides a novel mechanism for the regulation of CREB-dependent gene expression. Cell Mol Life Sci 2023;80:228. https://doi.org/10.1007/s00018-023-04876-8.
[191] Stefurak T, Mikulis D, Mayberg H, Lang AE, Hevenor S, Pahapill P, et al. Deep brain stimulation for Parkinson's disease dissociates mood and motor circuits: a functional MRI case study. Mov Disord 2003;18:1508–16. https://doi.org/10.1002/mds.10593.
[192] Skogseid IM, Ramm-Pettersen J, Volkmann J, Kerty E, Dietrichs E, Røste GK. Good long-term efficacy of pallidal stimulation in cervical dystonia: a prospective, observer-blinded study. Eur J Neurol 2012;19:610–5. https://doi.org/10.1111/j.1468-1331.2011.03591.x.
[193] Fenoy AJ, Schulz PE, Selvaraj S, Burrows CL, Zunta-Soares G, Durkin K, et al. A longitudinal study on deep brain stimulation of the medial forebrain bundle for treatment-resistant depression. Transl Psychiatry 2018;8:111. https://doi.org/10.1038/s41398-018-0160-4.

[194] Crowell AL, Riva-Posse P, Holtzheimer PE, Garlow SJ, Kelley ME, Gross RE, et al. Long-Term Outcomes of Subcallosal Cingulate Deep Brain Stimulation for Treatment-Resistant Depression. Am J Psychiatry 2019;176:949–56. https://doi.org/10.1176/appi.ajp.2019.18121427.
[195] Gadot R, Najera R, Hirani S, Anand A, Storch E, Goodman WK, et al. Efficacy of deep brain stimulation for treatment-resistant obsessive-compulsive disorder: systematic review and meta-analysis. J Neurol Neurosurg Psychiatry 2022:jnnp-2021-328738. https://doi.org/10.1136/jnnp-2021-328738.
[196] Mohan UR, Watrous AJ, Miller JF, Lega BC, Sperling MR, Worrell GA, et al. The effects of direct brain stimulation in humans depend on frequency, amplitude, and white-matter proximity. Brain Stimul 2020;13:1183–95. https://doi.org/10.1016/j.brs.2020.05.009.
[197] Tufail Y, Yoshihiro A, Pati S, Li MM, Tyler WJ. Ultrasonic neuromodulation by brain stimulation with transcranial ultrasound. Nat Protoc 2011;6:1453–70. https://doi.org/10.1038/nprot.2011.371.
[198] Ai L, Bansal P, Mueller JK, Legon W. Effects of transcranial focused ultrasound on human primary motor cortex using 7T fMRI: a pilot study. BMC Neurosci 2018;19:56. https://doi.org/10.1186/s12868-018-0456-6.
[199] Legon W, Ai L, Bansal P, Mueller JK. Neuromodulation with single-element transcranial focused ultrasound in human thalamus. Hum Brain Mapp 2018;39:1995–2006. https://doi.org/10.1002/hbm.23981.

**Figure legends**

**Fig. 1. Stimulation paradigms, temporal patterns, and distributions.** A-C) Stimulation paradigms for: 1 Hz continuous, 10 Hz continuous, and 10 Hz (or 100 Hz) discontinuous conditioning stimulation, respectively. Grey bands represent pre- and post-conditioning periods, while black bands represent intervals of conditioning stimulation. Note that for discontinuous stimulation paradigms (C) the conditioning period consists of alternating stimulation epochs (black bands) and rest intervals (grey bands). Rest intervals (10 Hz = 101.25 sec each, 100 Hz = 111.372 sec each) have probe trials at 0.1 Hz. D-E) Example of perfectly regular stimulation (D), with all ISIs equal (E). F-G) Example of slightly irregular stimulation (F), where ISIs have a Gaussian distribution (G). H-I) Example of highly irregular stimulation (H), where ISIs have a Poisson distribution (I). Note that the times shown in panels E-I are based on 1 Hz stimulation (10 Hz or 100 Hz stimulation was identical in pattern, but 10 or 100 times shorter in duration, respectively).

**Fig. 2. Efficacy of our CCI model for mTBI.** A-D) Data for: (A) righting reflex, (B) intracellular calcium concentration, (C) input resistance, and (D) membrane potential; in control (black), sham (blue) and mTBI (red) groups. Values are means ± SEM. n = number of observations/group. *$p < 0.05$, Fisher's LSD tests; #$p < 0.017$, Dunn's tests.

**Fig. 3. Individual time plots of WC responses to highly irregular (CV=1.0) 1 Hz continuous conditioning stimulation.** A-C) Representative examples of: control (A), sham (B), and mTBI (C) responses. Black open circles = pre-/post-conditioning responses, black filled circles = conditioning responses, red dotted line = baseline. Numerical values = post/pre ratios. Plasticity

outcome = (LTD, NC or LTP). Insets: PSP waveforms averaged over the last 5 min of pre- (grey) or post- (orange) conditioning (scale bars: 5 mV, 50 ms).

**Fig. 4. Continuous 1 Hz conditioning stimulation induces a net LTD response for every condition except one—highly irregular stimulation in mTBI rats shows a net LTP response.** A-C) Mean time plots for control groups with: perfectly regular (A), slightly irregular (B), and highly irregular (C) stimulation. Inset text: mean post/pre ratio ± SEM, p-values (*t* test comparing the last 5 min of pre- vs. post- conditioning), and the number of cells (n=). Red dashed line = baseline. D-F) Mean time plots for mTBI groups. G-H) Cumulative probability plots. Data steps falling: in the grey region show NC, to the left show LTD, and to the right show LTP. In control groups (G), temporal pattern had no appreciable effect on plasticity outcome (curves overlap); but in mTBI groups (H), highly irregular stimulation resulted in significant potentiation. #$p < 0.017$, Dunn's tests. I) Cumulative probability plots showing the effect of highly irregular stimulation in control sham, and mTBI groups. Note the rightward shift indicating potentiation in the mTBI group relative to control and sham rats. #$p < 0.017$, Dunn's tests.

**Fig. 5. Continuous 10 Hz (compared to 1 Hz) conditioning stimulation produces a rapid rundown in PSP amplitudes, is less likely to result in net LTD in controls, and more likely to result in net LTP after mTBI.** A-C) Mean time plots for control groups with perfectly regular (A), slightly irregular (B), and highly irregular (C) stimulation. Inset text: mean post/pre ratio ± SEM, p-values (*t* test comparing the last 5 min of pre- vs. post- conditioning), and the number of cells (n). Red dashed line = baseline. D-F) Mean time plots for mTBI groups. G-H) cumulative probability plots of post/pre ratios for control groups (G) and mTBI groups (H). Note that temporal pattern has no effect on plasticity outcome in control groups (curves in G overlap), while in mTBI

groups (H) the curves for perfectly regular and highly irregular stimulation are shifted to the right indicating potentiation. *$p < 0.05$, Kruskal-Wallis test with Dunn's tests. I) cumulative probability plot showing the effect of highly irregular stimulation in control, sham, and mTBI groups. Note the rightward shift indicating potentiation in mTBI relative to control and sham groups. *$p < 0.05$, Kruskal-Wallis test with Dunn's tests.

**Fig. 6. Discontinuous 10 Hz conditioning stimulation primarily induced a net LTD, except for slightly irregular stimulation in controls and highly irregular stimulation in mTBI rats.** A-C) Mean time plots for control groups with perfectly regular (A), slightly irregular (B), and highly irregular (C) stimulation. Note the eight rest periods (consisting of 0.1 Hz probe trials = yellow circles), evenly spaced between the nine stimulation epochs (black circles). Inset text: mean post/pre ratio ± SEM, p-values (*t* test comparing the last 5 min of pre- vs. post- conditioning), and the number of cells (n). Red dashed line = baseline. D-F) Mean time plots for mTBI groups. G-I) Cumulative probability plots of post/pre ratios for control groups (G) and mTBI groups (H). In control groups (G), note the rightward shift (potentiation) for slightly irregular stimulation, and leftward shift (depression) for highly irregular stimulation. In mTBI groups (H), there is a rightward shift (potentiation) for highly irregular stimulation. *$p < 0.05$, Kruskal-Wallis test with Dunn's tests. I) cumulative probability plot showing the effect of highly irregular stimulation in control, sham, and mTBI groups. Note the rightward shift indicating potentiation in mTBI relative to both control and sham groups. *$p < 0.05$, Kruskal-Wallis test with Dunn's tests.

**Fig. 7. Discontinuous 100 Hz conditioning stimulation shows little net plasticity, although highly irregular stimulation in controls results in net LTD, and slightly irregular stimulation in mTBI rats produces net LTP.** A-C) Mean time plots for control groups with perfectly regular

(A), slightly irregular (B), and highly irregular (C) stimulation. Inset text: mean post/pre ratio ± SEM, p-values (*t* test comparing the last 5 min of pre- vs. post- conditioning), and the number of cells (n). Red dashed line = baseline. Grey bars indicate the period during which conditioning stimulation was applied. Note that data for conditioning stimulation epochs are not shown because the brevity of ISIs precluded measurement of most PSP peak amplitudes. Yellow symbols represent probe trials (at 0.1 Hz) between stimulation epochs. D-F) Mean time plots for mTBI groups. G-H) cumulative probability plots of post/pre ratios for control (G) and mTBI groups (H). Note comparisons within control (G) and mTBI groups (H) showed no significant difference between the three temporal patterns of stimulation (control, p = 0.17; mTBI, p = 0.93; Kruskal-Wallis tests). I) cumulative probability plot showing the effect of highly irregular 100 Hz conditioning stimulation in control and mTBI groups. Note that for 100 Hz discontinuous, unlike 1 Hz continuous, 10 Hz continuous, and 10 Hz discontinuous highly irregular stimulation, there was no significant difference in plasticity outcomes for control verses mTBI groups ($p = 0.28$, *t* test).

**Fig. 8. For 1 Hz continuous highly irregular conditioning stimulation, the individual kinetic profile of conditioning response amplitudes is predictive of plasticity outcome.** A-C) Individual time plots of conditioning period normalized PSP peak amplitudes, for representative control (A), sham (B), and mTBI (C) examples. Tan symbols show the average of normalized PSP peak amplitudes for the last 5 min of the pre-conditioning baseline (left), and the last 5 min of the post-conditioning response (right). For each time plot we calculated the exponential best fit (purple dotted line) and linear best fit (yellow solid line) to obtain the exponential and linear slopes, respectively. D-E) Plots of post/pre ratio (plasticity outcome) verses exponential slope (D), and linear slope (E), respectively (control, n = 17; sham, n = 16; mTBI, n = 17). r = correlation

coefficient. Note that the conditioning slope shows a significant positive correlation for an exponential fit only in the control and sham groups (D), and a linear fit only in mTBI group (E). *$p < 0.05$, simple linear regression. F) Normalized PSP peak amplitude during conditioning: Ave (average of all data points), Int (initial 10% of data points averaged), and Fin (final 10% of data points averaged). Values are mean ± SEM. Note that normalized PSP peak amplitudes during conditioning are significantly greater in mTBI vs. control group. #$p < 0.017$, Dunn's test. $t$ = trend ($p = 0.019$, Dunn's test). G-I) Plots of post/pre ratio (plasticity outcome) vs. normalized PSP peak amplitude: average (G), initial (H), and final (I) values. Note that while all normalized conditioning amplitudes (average, initial and final) are significantly correlated with plasticity outcome in the mTBI group, only the average and final values are correlated with plasticity outcome in the control and sham groups. *$p < 0.05$, simple linear regression.

**Fig. 9. For 10 Hz continuous highly irregular conditioning stimulation, the individual kinetic profile of conditioning response amplitudes was not predictive of plasticity outcome.** A-C) Individual time plots of conditioning period normalized PSP peak amplitudes, for representative control (A), sham (B), and mTBI (C) examples. Tan symbols show the average normalized PSP peak amplitudes for the last 5 min of the pre-conditioning baseline (left), and the last 5 min of the post-conditioning response (right). For each time plot we calculated the exponential best fit (purple dotted line) and linear best fit (yellow solid line) to obtain the exponential and linear slopes, respectively. D-E) Plots of post/pre ratio (plasticity outcome) verses exponential slope (D), and linear slope (E), respectively (control, n = 15; sham, n = 17; mTBI, n = 21). r = correlation coefficient. Note that post/pre ratio (plasticity outcome) shows no significant correlation with either exponential or linear slope (in controls: $p = 0.44$, $p = 0.38$, respectively; in shams: $p = 0.18$, $p = 0.96$, respectively; in mTBI: $p = 0.34$, $p = 0.37$, respectively; simple linear regressions). F)

Normalized PSP peak amplitude: average (Ave), initial (Int), and final (Fin) values. Values are mean ± SEM. #$p$ < 0.017, Dunn's test. G-I) Plots of post/pre ratio (plasticity outcome) vs. normalized PSP peak amplitude: average (G), initial (H), and final (I) values. Note that post/pre ratio (plasticity outcome) is not significantly correlated with normalized PSP amplitude in any treatment group (control, sham, or mTBI).

**Fig. 10. For 10 Hz discontinuous highly irregular conditioning stimulation, conditioning period amplitudes have: slopes (exponential and linear) that show significant negative correlations with plasticity outcome in control and sham, but not mTBI groups; and magnitudes (average, initial and final) that show significant positive correlations with plasticity outcome in mTBI groups, but not control or sham groups.** A-C) Individual time plots of conditioning period normalized peak amplitudes for a representative control (A), sham (B), and mTBI (C) example. Note that only the first, fifth and ninth conditioning epochs are shown (the full conditioning period consists of 9 stimulation epochs separated by 8 equal rest intervals). Tan symbols represent the average of normalized PSP peak amplitudes for (from left to right): the last 5 min of pre-conditioning and the first rest interval (left panel), the fourth and fifth rest intervals (center panel), and the eighth rest interval and the last 5 min of post-conditioning (right panel). For each panel we calculated the exponential best fit (purple dotted line) and linear best fit (yellow solid line) to obtain the exponential and linear slopes. D-E) Plots of post/pre ratio (plasticity outcome) vs. conditioning response slope (averaged over all 9 stimulation epochs) for exponential (D), and linear (E) best fits, respectively (control: n = 17; sham: n = 16, mTBI: n = 16). r = correlation coefficient. Note that the conditioning slopes (exponential and linear) show a significant negative correlation with plasticity outcome in control ($p$ < 0.001 and $p$ <0.001, respectively) and sham ($p$ = 0.04 and $p$ = 0.02, respectively) groups, but not mTBI ($p$ = 0.84 and

$p$ = 0.64, respectively) groups. *$p$ < 0.05, simple linear regression. F) Normalized PSP peak amplitude: average (Ave), initial (Int), and final (Fin) values. Values are mean ± SEM. Note that these values are similar for all treatment groups (control, sham, and mTBI). G-I) Plots of post/pre ratio (plasticity outcome) verse normalized PSP peak amplitude: average (G), initial (H), and final (I) values. Note that all conditioning response amplitudes show a significant positive correlation with plasticity outcome in the mTBI group (average: $p$ = 0.03, initial: $p$ = 0.04, final: $p$ = 0.03), but not the control (average: $p$ = 0.71, initial: $p$ = 0.17, final: $p$ = 0.69) or sham (average: $p$ = 0.35, initial: $p$ = 0.24, final: $p$ = 0.44) groups.

**Fig. 11. Individual whole-cell and field potential recordings made in parallel show a significant correlation in plasticity outcomes.** A-B) Individual time plots of WC (A) and FP (B) responses to 1 Hz continuous conditioning stimulation (black open circles = pre-/post-conditioning period responses, black filled circles = conditioning period responses). Inset text: shows mean post/pre ratios ± SEM, with the corresponding plasticity outcome (LTD, NC or LTP) shown in parentheses. Inset figure: averaged response waveforms for the last 5 min of pre- (grey) and post- (orange) conditioning (scale bars: WC = 5 mV, 50 ms; FP = 50 μV, 10 ms). WC and FP time plots shown on the same row were recorded in parallel from the same slice. C-D) Individual time plots of WC (C) and FP (D) responses to 10 Hz continuous conditioning stimulation. E-F) Individual time plots of WC (E) and FP (F) responses to 10 Hz discontinuous conditioning stimulation. Yellow symbols during conditioning represent probe trials (at 0.1 Hz) between stimulus epochs. All examples (A-F) depict control data. G-H) WC and FP recordings made simultaneously yield post/pre ratios (plasticity outcomes) which are highly correlated regardless of treatment group (G): control (n = 50), sham (n = 26), or mTBI (n = 69); or temporal pattern (H): CV 0.0 (n = 25), CV

0.2 (n=43), or CV 1.0 (n=77). Solid lines represent a linear best fit; r = correlation coefficient; ***$p < 0.001$, simple linear regression.

**Supp. Fig. 1. Significant changes in shape indices were induced only by a few stimulation paradigms, and were dependent on treatment group (control, sham, mTBI), temporal pattern (CV 0.0, CV 0.2, CV 1.0), and plasticity outcome (LTD, LTP, NC).** A) Example PSP waveforms averaged over the last 5 min of pre- (grey) or post- (orange) conditioning. Red dotted line = baseline. Peak / solid arrows = PSP peak amplitude, RT = rise time (10-90% of peak amplitude), DT = decay time (90-10% of peak amplitude), arrowheads indicate 10-90% bounds of RT or DT, HW / open arrows = half width (at half height). B-D) Shape indices before and after 1 Hz continuous highly irregular conditioning stimulation for: all cells (B), only cells showing LTD (C), only cells showing LTP (D). E-G) Shape indices before and after 100 Hz discontinuous highly irregular conditioning stimulation for: all cells (E), only cells showing LTD (F), only cells showing LTP (G). H-J) Shape indices before and after 100 Hz discontinuous slightly irregular conditioning stimulation for: all cells (H), only cells showing LTD (I), only cells showing LTP (J). *$p < 0.05$, **$p < 0.01$, paired *t*-test. n = number of cells for each paired group pre- (solid bars) and post- (open bars) conditioning for the same cells.

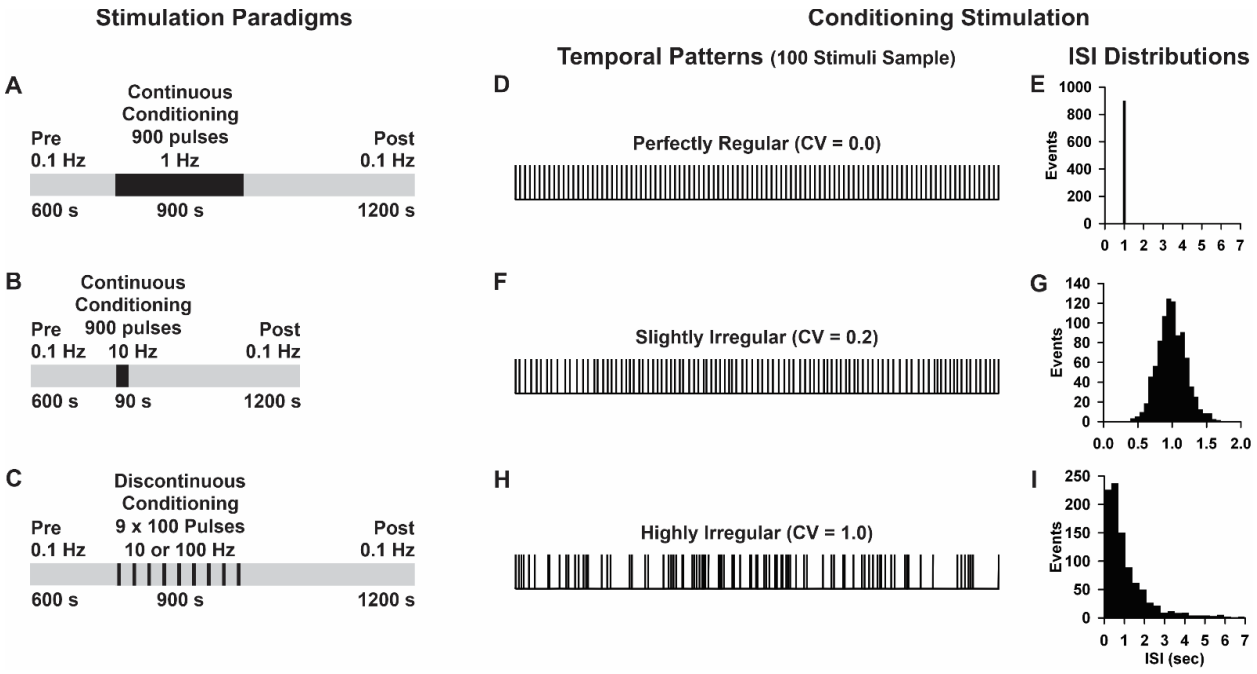
Stimulation Paradigms
Conditioning Stimulation
Temporal Patterns (100 Stimuli Sample)
ISI Distributions
A
Continuous Conditioning
Pre 0.1 Hz
900 pulses 1 Hz
Post 0.1 Hz
600 s
900 s
1200 s
B
Continuous Conditioning
Pre 0.1 Hz
900 pulses 10 Hz
Post 0.1 Hz
600 s
90 s
1200 s
C
Discontinuous Conditioning
Pre 0.1 Hz
9 x 100 Pulses 10 or 100 Hz
Post 0.1 Hz
600 s
900 s
1200 s
D
Perfectly Regular (CV = 0.0)
E
F
Slightly Irregular (CV = 0.2)
G
H
Highly Irregular (CV = 1.0)
I
Events
ISI (sec)

Fig. 1

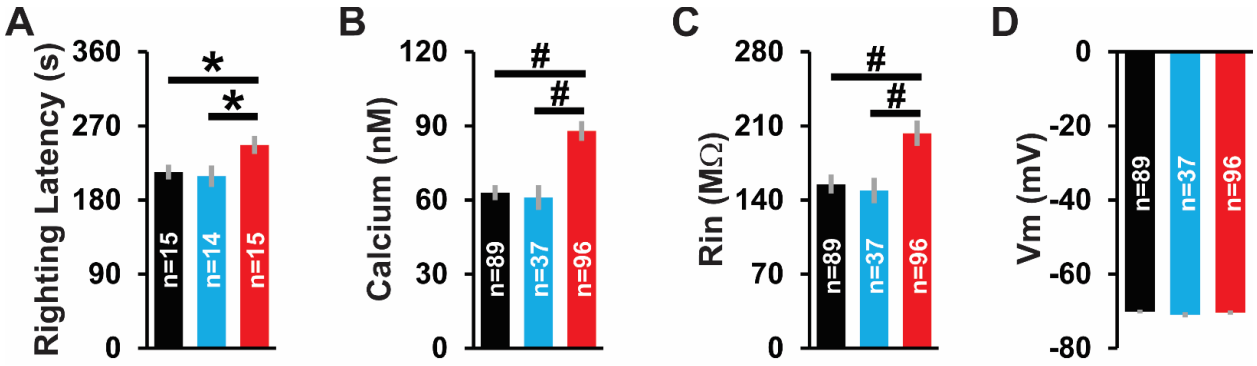
A
Righting Latency (s)
360
270
180
90
0
*
*
n=15
n=14
n=15
B
Calcium (nM)
120
90
60
30
0
#
#
n=89
n=37
n=96
C
Rin (MΩ)
280
210
140
70
0
#
#
n=89
n=37
n=96
D
Vm (mV)
0
-20
-40
-60
-80
n=89
n=37
n=96

Fig. 2

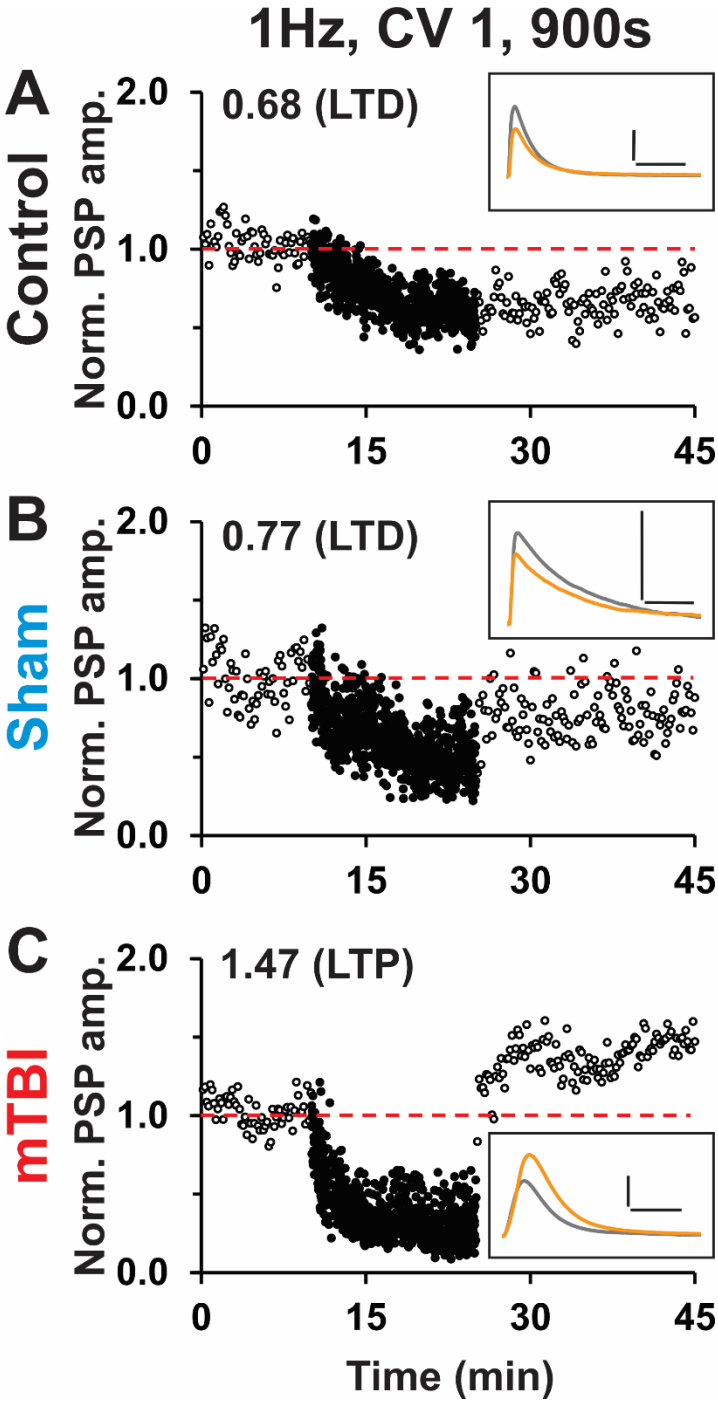
1Hz, CV 1, 900s
A
Control
0.68 (LTD)
B
Sham
0.77 (LTD)
C
mTBI
1.47 (LTP)
Norm. PSP amp.
2.0
1.0
0.0
0
15
30
45
Time (min)

Fig. 3

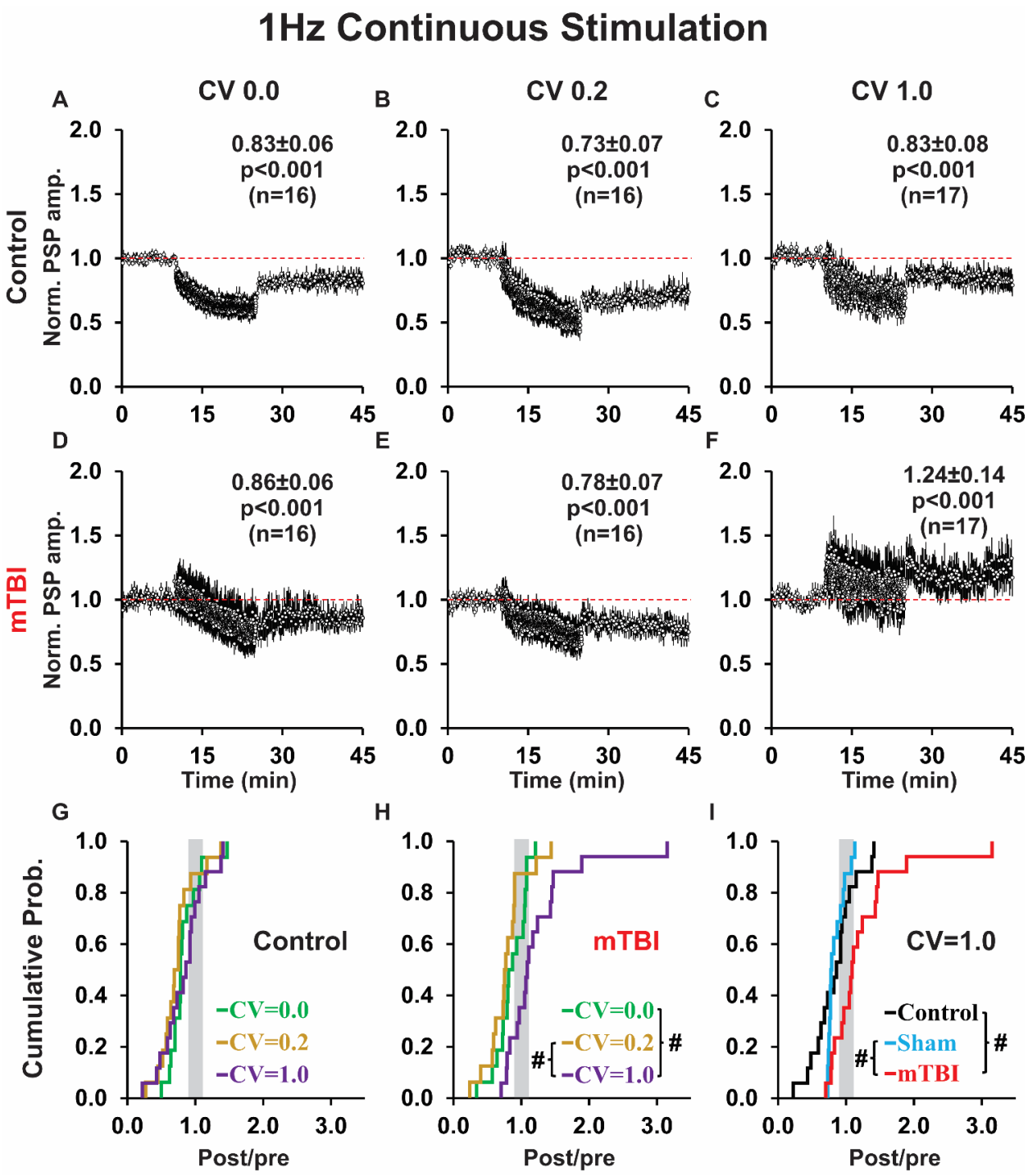
1Hz Continuous Stimulation
A
CV 0.0
0.83±0.06
p<0.001
(n=16)
B
CV 0.2
0.73±0.07
p<0.001
(n=16)
C
CV 1.0
0.83±0.08
p<0.001
(n=17)
Control
Norm. PSP amp.
D
0.86±0.06
p<0.001
(n=16)
E
0.78±0.07
p<0.001
(n=16)
F
1.24±0.14
p<0.001
(n=17)
mTBI
Norm. PSP amp.
Time (min)
G
Control
-CV=0.0
-CV=0.2
-CV=1.0
H
mTBI
-CV=0.0
-CV=0.2
-CV=1.0
#
I
CV=1.0
-Control
-Sham
-mTBI
#
Cumulative Prob.
Post/pre

Fig .4

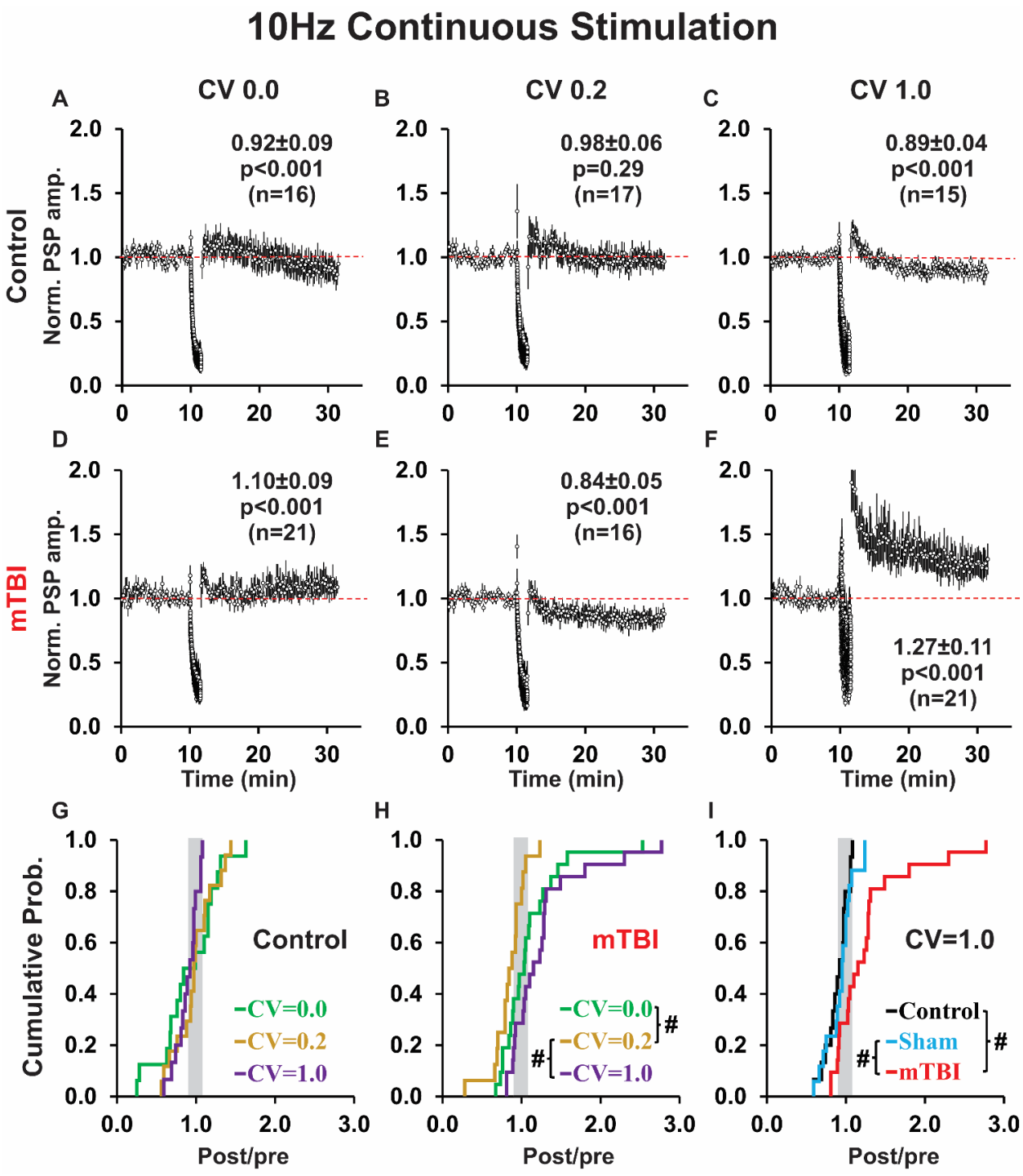
10Hz Continuous Stimulation
A
CV 0.0
0.92±0.09
p<0.001
(n=16)
B
CV 0.2
0.98±0.06
p=0.29
(n=17)
C
CV 1.0
0.89±0.04
p<0.001
(n=15)
Control
Norm. PSP amp.
D
1.10±0.09
p<0.001
(n=21)
E
0.84±0.05
p<0.001
(n=16)
F
1.27±0.11
p<0.001
(n=21)
mTBI
Time (min)
G
Control
CV=0.0
CV=0.2
CV=1.0
H
mTBI
CV=0.0
CV=0.2
CV=1.0
#
I
CV=1.0
Control
Sham
mTBI
Cumulative Prob.
Post/pre

Fig. 5

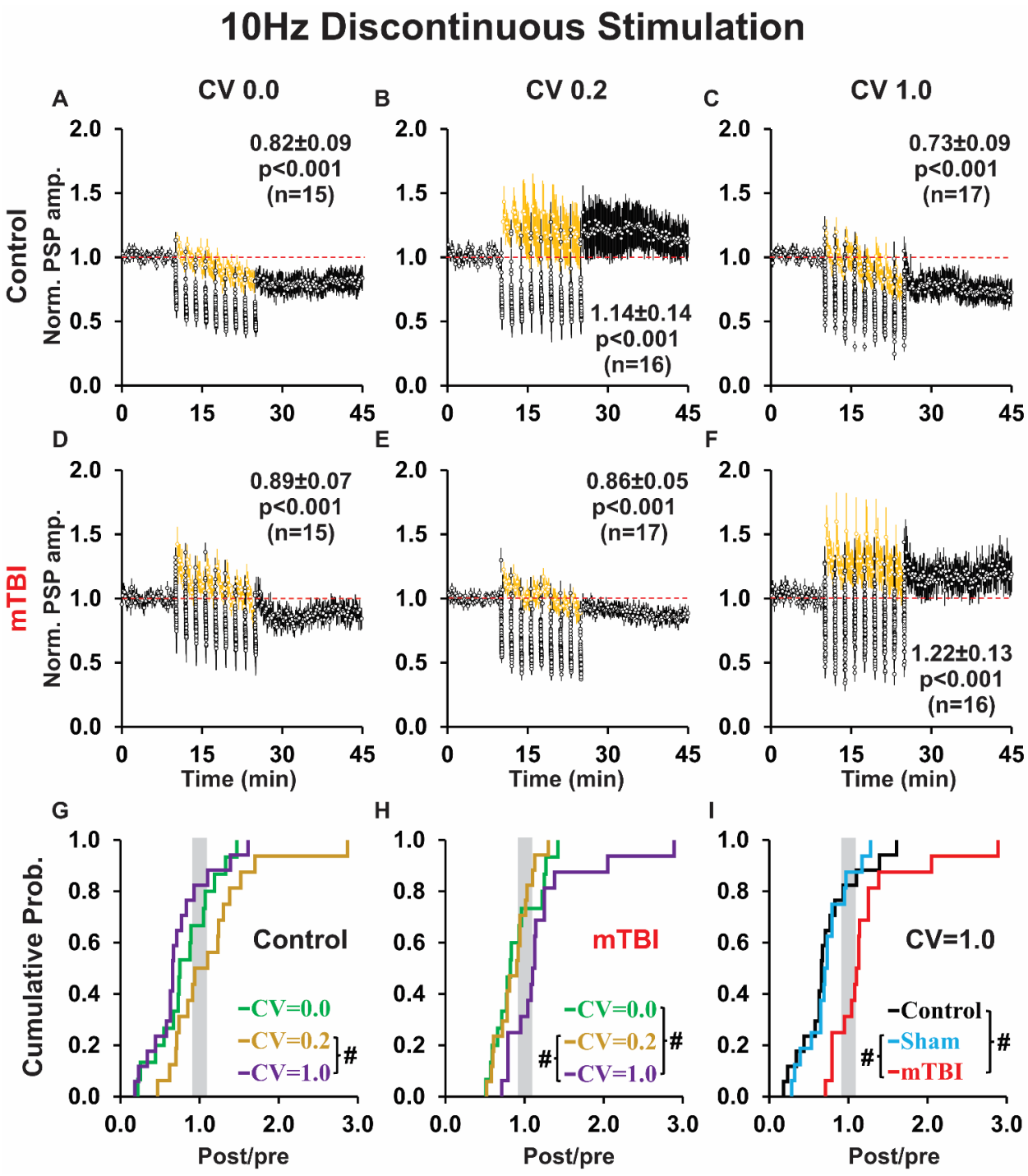
10Hz Discontinuous Stimulation
A
CV 0.0
B
CV 0.2
C
CV 1.0
Control
Norm. PSP amp.
0.82±0.09
p<0.001
(n=15)
1.14±0.14
p<0.001
(n=16)
0.73±0.09
p<0.001
(n=17)
D
E
F
mTBI
0.89±0.07
p<0.001
(n=15)
0.86±0.05
p<0.001
(n=17)
1.22±0.13
p<0.001
(n=16)
Time (min)
G
H
I
Cumulative Prob.
Control
CV=0.0
CV=0.2
CV=1.0
#
mTBI
CV=1.0
Control
Sham
mTBI
Post/pre

Fig. 6

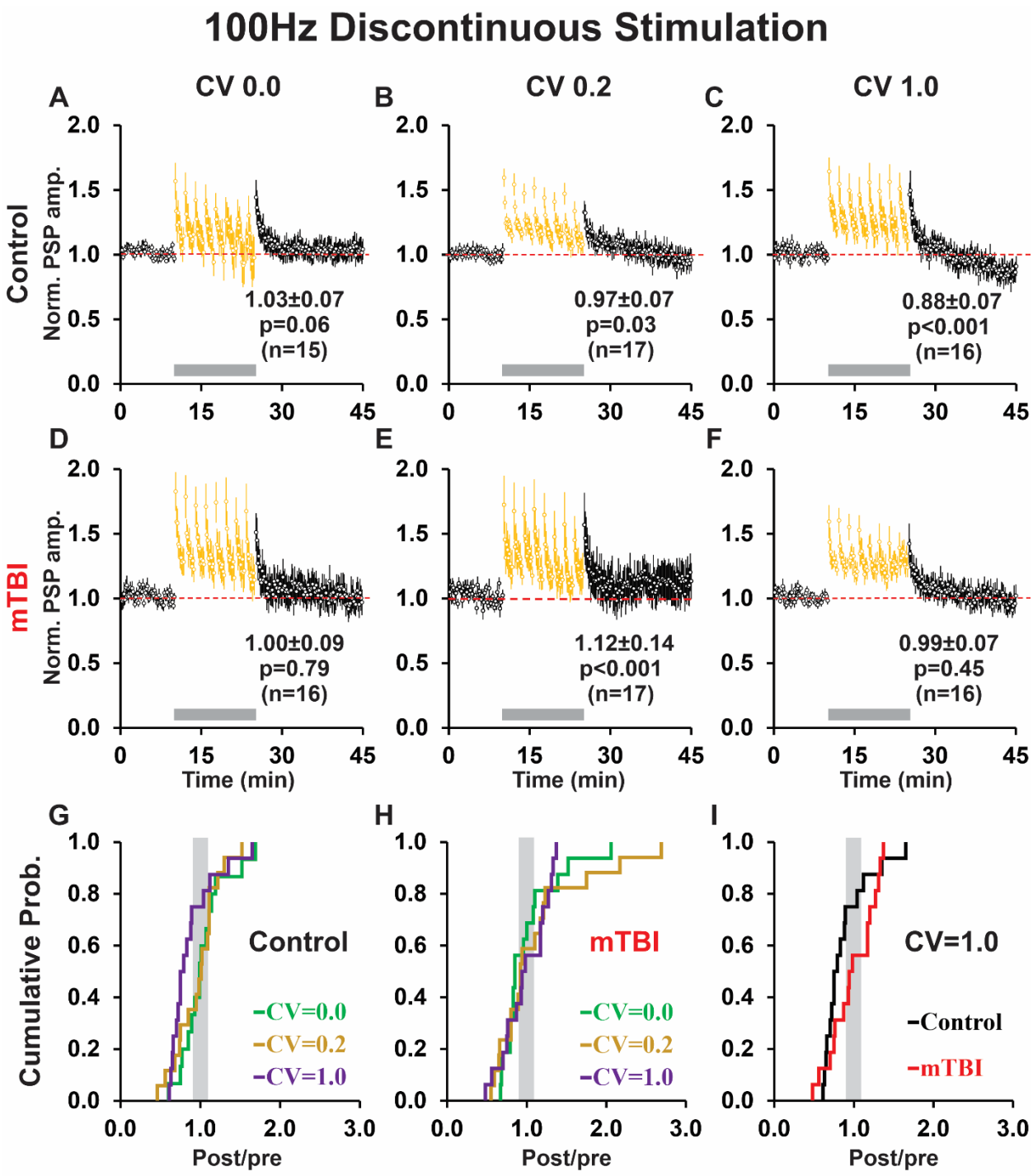
100Hz Discontinuous Stimulation
A
CV 0.0
B
CV 0.2
C
CV 1.0
Control
Norm. PSP amp.
1.03±0.07
p=0.06
(n=15)
0.97±0.07
p=0.03
(n=17)
0.88±0.07
p<0.001
(n=16)
D
E
F
mTBI
1.00±0.09
p=0.79
(n=16)
1.12±0.14
p<0.001
(n=17)
0.99±0.07
p=0.45
(n=16)
Time (min)
G
H
I
Cumulative Prob.
Control
-CV=0.0
-CV=0.2
-CV=1.0
mTBI
CV=1.0
-Control
-mTBI
Post/pre

Fig. 7

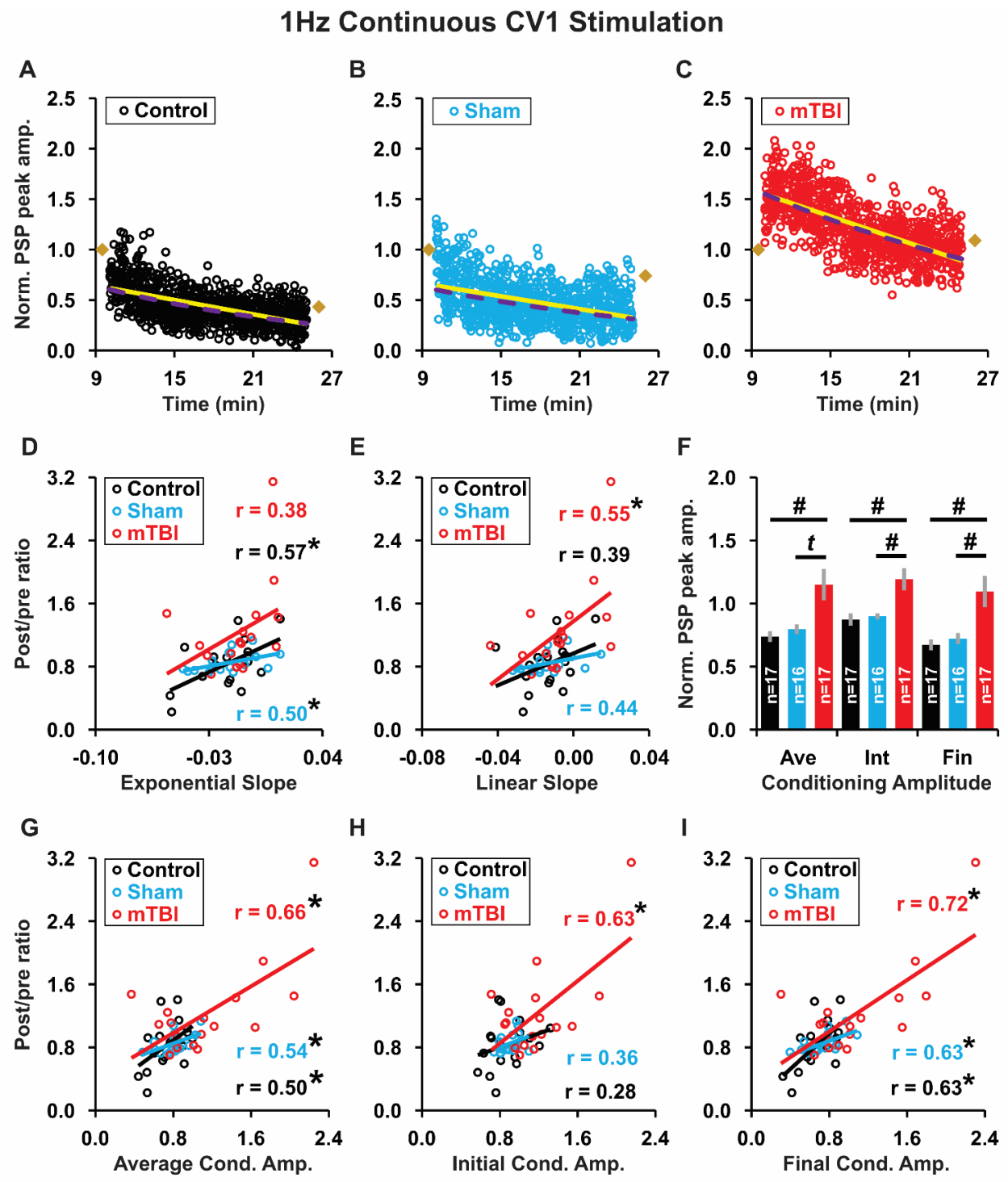
1Hz Continuous CV1 Stimulation
A
B
C
Control
Sham
mTBI
Norm. PSP peak amp.
Time (min)
D
E
F
Post/pre ratio
Exponential Slope
Linear Slope
Norm. PSP peak amp.
Conditioning Amplitude
Ave
Int
Fin
r = 0.38
r = 0.57*
r = 0.50*
r = 0.55*
r = 0.39
r = 0.44
n=17
n=16
G
H
I
Average Cond. Amp.
Initial Cond. Amp.
Final Cond. Amp.
r = 0.66*
r = 0.54*
r = 0.50*
r = 0.63*
r = 0.36
r = 0.28
r = 0.72*
r = 0.63*
r = 0.63*

Fig. 8

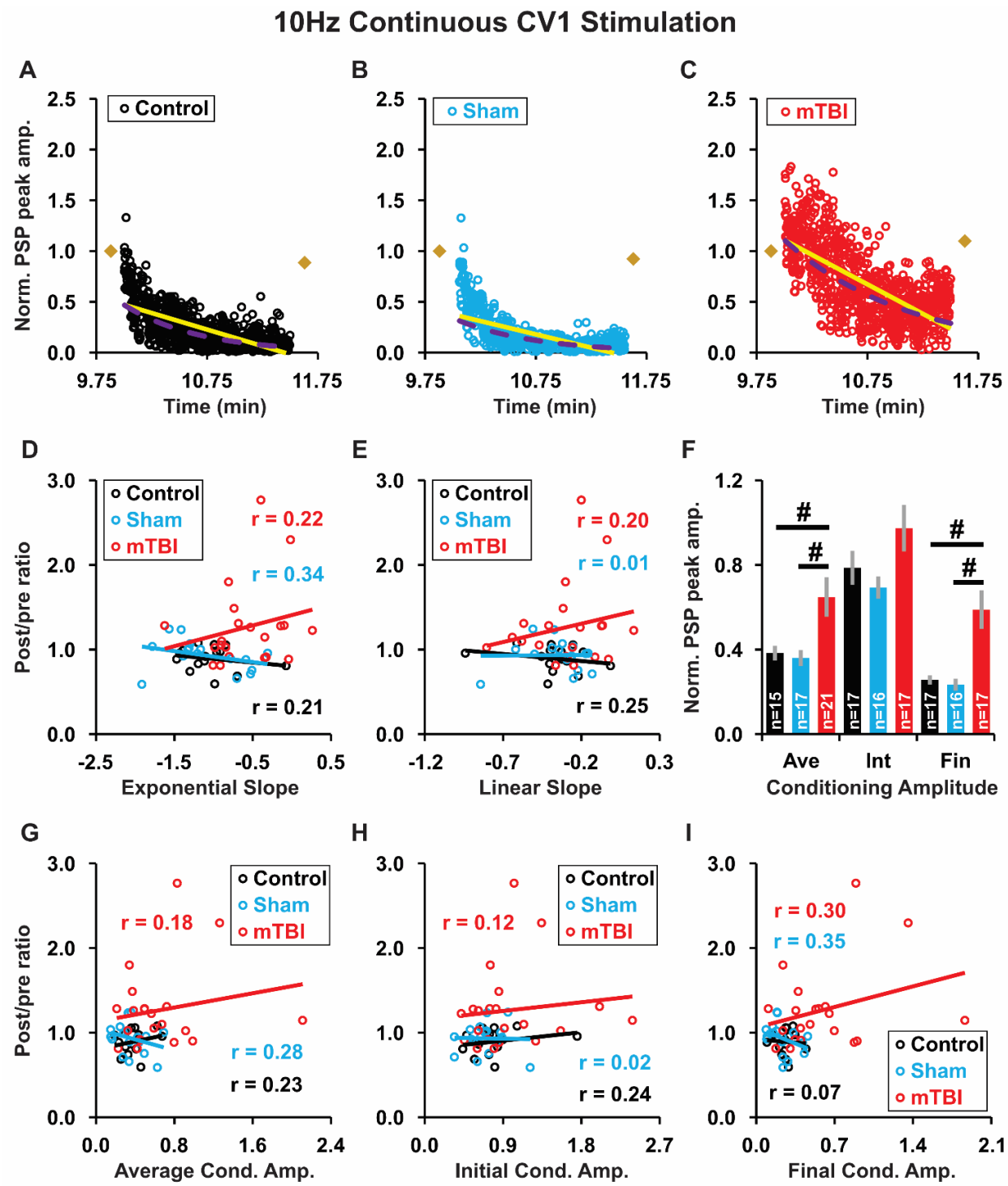
10Hz Continuous CV1 Stimulation
A
B
C
Control
Sham
mTBI
Norm. PSP peak amp.
Time (min)
D
E
F
Post/pre ratio
Exponential Slope
Linear Slope
Norm. PSP peak amp.
Conditioning Amplitude
Ave
Int
Fin
r = 0.22
r = 0.34
r = 0.21
r = 0.20
r = 0.01
r = 0.25
n=15
n=17
n=21
n=17
n=16
n=17
n=17
n=16
n=17
G
H
I
Average Cond. Amp.
Initial Cond. Amp.
Final Cond. Amp.
r = 0.18
r = 0.28
r = 0.23
r = 0.12
r = 0.02
r = 0.24
r = 0.30
r = 0.35
r = 0.07

Fig. 9

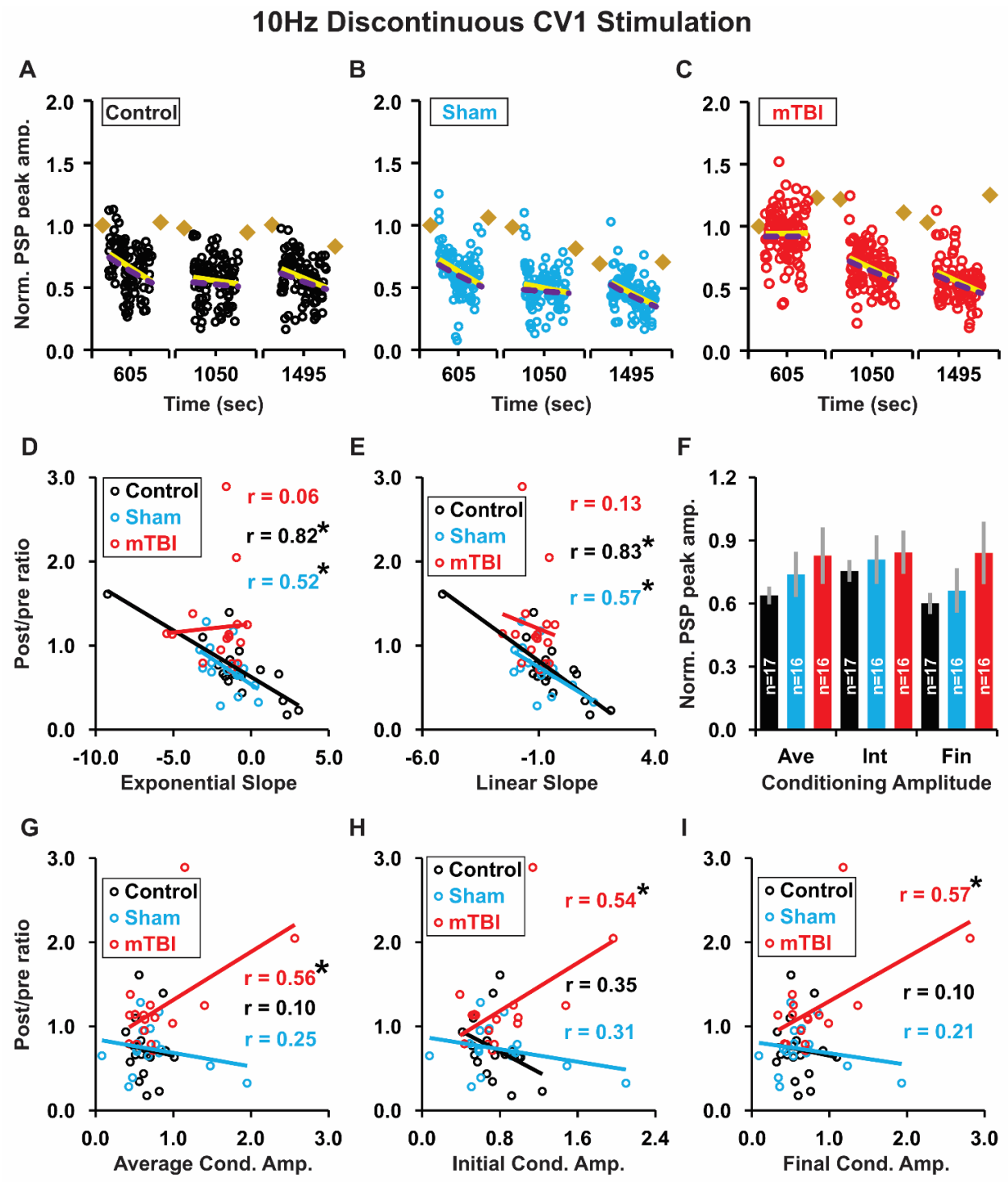
10Hz Discontinuous CV1 Stimulation
A
B
C
Control
Sham
mTBI
Norm. PSP peak amp.
Time (sec)
605
1050
1495
D
E
F
Post/pre ratio
Exponential Slope
Linear Slope
Norm. PSP peak amp.
Conditioning Amplitude
Ave
Int
Fin
r = 0.06
r = 0.82*
r = 0.52*
r = 0.13
r = 0.83*
r = 0.57*
n=17
n=16
G
H
I
Average Cond. Amp.
Initial Cond. Amp.
Final Cond. Amp.
r = 0.56*
r = 0.10
r = 0.25
r = 0.54*
r = 0.35
r = 0.31
r = 0.57*
r = 0.10
r = 0.21

Fig. 10

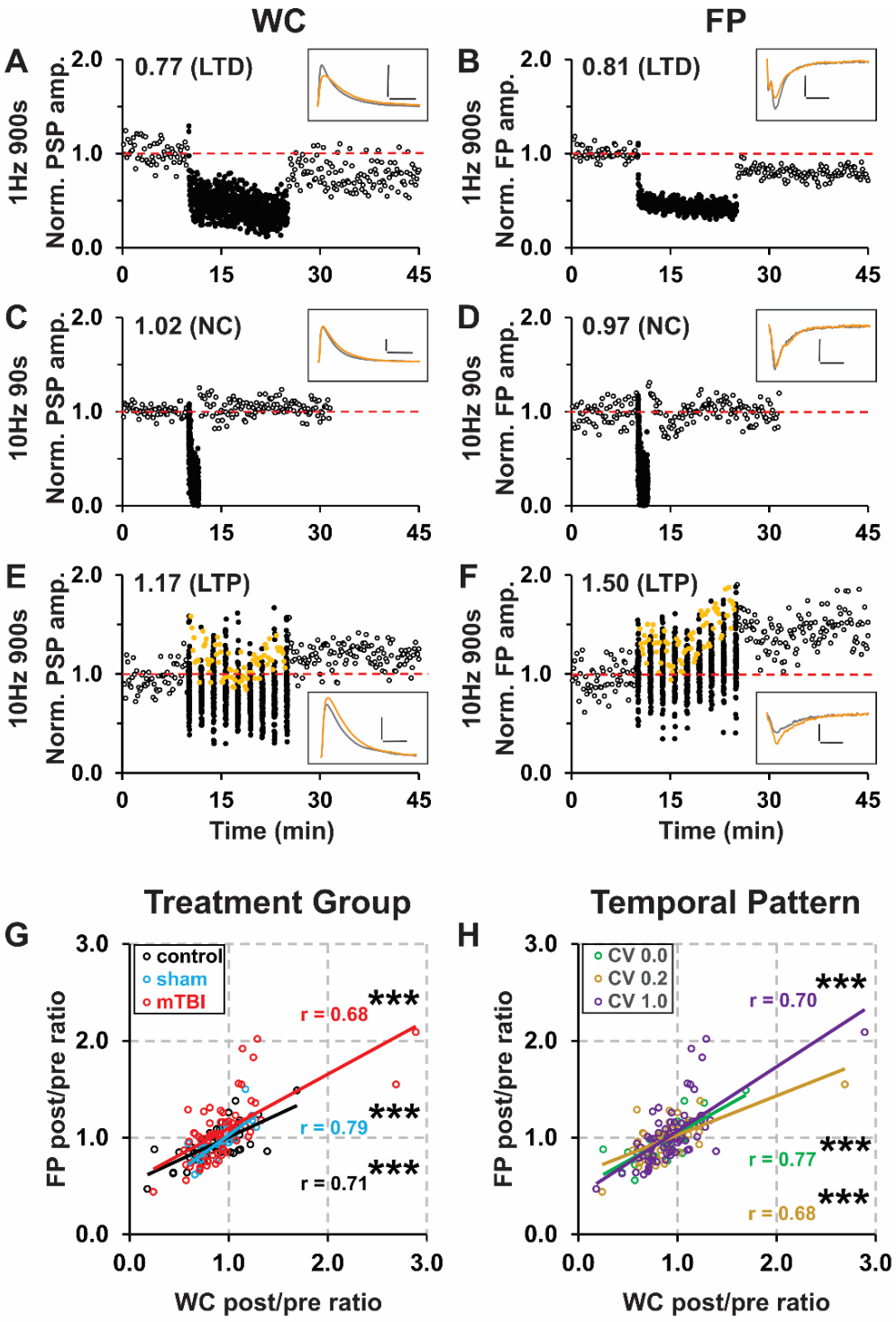
WC
FP
A
0.77 (LTD)
1Hz 900s
Norm. PSP amp.
B
0.81 (LTD)
1Hz 900s
Norm. FP amp.
C
1.02 (NC)
10Hz 90s
Norm. PSP amp.
D
0.97 (NC)
10Hz 90s
Norm. FP amp.
E
1.17 (LTP)
10Hz 900s
Norm. PSP amp.
F
1.50 (LTP)
10Hz 900s
Norm. FP amp.
Time (min)
Treatment Group
G
control
sham
mTBI
r = 0.68
r = 0.79
r = 0.71
***
FP post/pre ratio
WC post/pre ratio
Temporal Pattern
H
CV 0.0
CV 0.2
CV 1.0
r = 0.70
r = 0.77
r = 0.68

Fig. 11

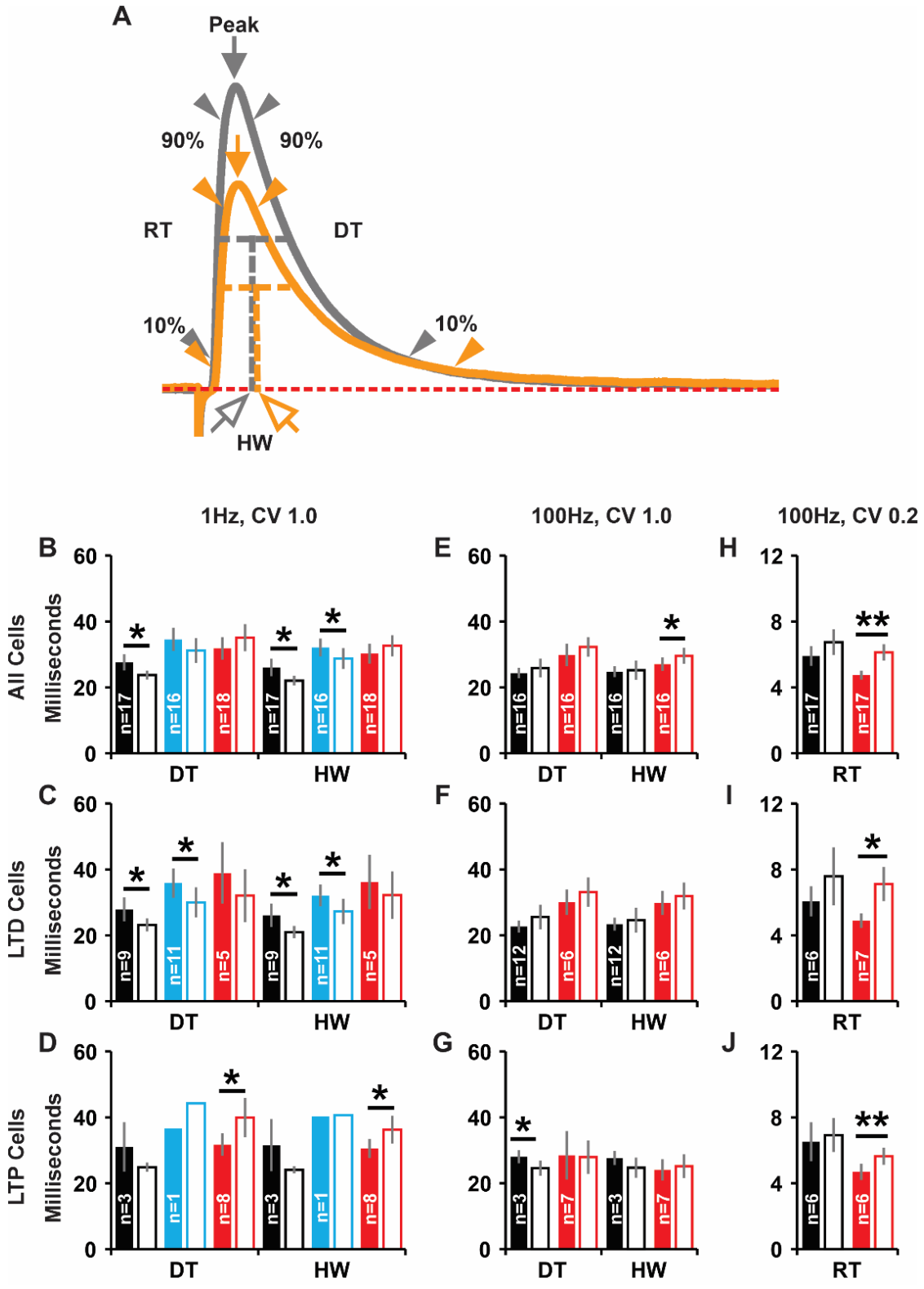
A
Peak
90%
90%
RT
DT
10%
10%
HW
1Hz, CV 1.0
100Hz, CV 1.0
100Hz, CV 0.2
B
C
D
E
F
G
H
I
J
All Cells
LTD Cells
LTP Cells
Milliseconds
DT
HW
RT
n=17
n=16
n=18
n=9
n=11
n=5
n=3
n=1
n=8
n=12
n=6
n=7

Supp. Fig. 1